

Drivers of nitrogen and phosphorus dynamics in a groundwater-fed urban catchment revealed by high frequency monitoring

Liang Yu^{1,2}, Joachim C. Rozemeijer³, Hans Peter Broers⁴, Boris M. van Breukelen⁵, Jack J. Middelburg⁶, Maarten Ouboter², and Ype van der Velde¹

¹Faculty of Science, Vrije University Amsterdam, 1181HV, Amsterdam, the Netherlands

²Waternet Water Authority, 1096 AC, Amsterdam, the Netherlands

³Deltares, 3508 TC, Utrecht, the Netherlands

⁴TNO Geological Survey of the Netherlands, 3584 CB, Utrecht, the Netherlands

⁵Department of Water Management, Faculty of Civil Engineering and Geosciences, Delft University of Technology, Stevinweg 1, 2628 CN, Delft, the Netherlands

⁶Department of Earth Sciences, Faculty of Geosciences, Utrecht University, P.O. Box 80 021, 3508 TA, Utrecht, the Netherlands

Correspondence to: Liang Yu (xiaobaidrawing@gmail.com)

Abstract. Eutrophication of water bodies has been a problem causing severe degradation of water quality in cities. To gain mechanistic understanding of the temporal dynamics of nitrogen (N) and phosphorus (P) in a groundwater fed low-lying urban polder, we applied high frequency monitoring in Geuzenveld, a polder in the city of Amsterdam. The high frequency monitoring equipment was installed at the pumping station where water leaves the polder. From March 2016 to June 2017, total phosphorus (TP), ammonium (NH₄), turbidity, electrical conductivity (EC), and water temperature were measured at intervals smaller than 20 minutes. This paper discussed the results at three time scales: annual scale, rain event scale, and single pumping event scale. Mixing of upwelling groundwater (main source of N and P) and runoff from precipitation on pavements and roofs was the dominant hydrological process governing the temporal pattern of the EC, while N and P fluxes from the polder were also regulated by primary production and iron transformations. In our groundwater-seepage controlled catchment, NH₄ appeared to be the dominant form of N with surface water concentrations in the range of 2-6 mg N/L, which stems from production in an organic-rich subsurface. The concentrations of NH₄ in the surface water were governed by the mixing process in autumn and winter and were reduced down to 0.1 mg N/L during the algae growing season in spring. The depletion of dissolved NH₄ in spring suggests uptake by primary producers, consistent with high concentrations of chlorophyll-a, O₂, and suspended solids during this period. Total P and turbidity were high during winter (range 0.5-2.5 mg P/L and 200-1800 FNU, respectively) due to the release of P and reduced iron from anoxic sediment to the water column, where Fe²⁺ was rapidly oxidised and precipitated as iron oxides which contributed to turbidity. In the other seasons, P is retained in the sediment by sorption to precipitated iron oxides. Nitrogen is exported from the polder to the receiving waters throughout the whole year, mostly in the form of NH₄, but in the form of organic N in spring. P leaves the polder mainly during winter, primarily associated with Fe(OH)₃ colloids and as dissolved P. Based on this new understanding of the dynamics of N and P in this low lying urban catchment, we suggested management strategies that may effectively control and reduce eutrophication in urban polders and receiving downstream waters.

Keywords: Nitrogen and phosphorus dynamic, high frequency monitoring, benthic algae, iron chemistry, Amsterdam, groundwater seepage

1 Introduction

Eutrophication is one of the most notorious phenomena of water quality impairment in cities, caused by excess inputs of N and P. The identified sources of nutrients are from wastewater treatment plants, storm runoff, overflow of sewage systems, manure and fertilizer application in urban green areas and atmospheric deposition (Walsh et al., 2005; Kabenge et al., 2016; Toor et al., 2017; Yang & Toor, 2018; Putt et al., 2019). Recently, groundwater has been identified as another important source

42 of N and P in cities situated in low-lying deltas, where dissolved NH_4 and PO_4 in groundwater seep up into urban surface water
43 (Yu et al., 2018 & 2019). The upwelling nutrients in groundwater, originating from the organic rich delta subsurface, reaching
44 the surface water of cities and are transferred to downstream waters and eventually reach the coastal zones, where they may
45 induce harmful algal blooms or cause hypoxia along coastlines (He and Xu, 2015; Beusen et al., 2016; Le Moal et al., 2019).
46 Hence, it is of pivotal importance to understand N and P dynamics in the urban freshwater bodies in order to mitigate the input
47 of nutrients into the oceans (e.g. Nyenje, et al., 2010; Toor et al., Paerl et al., 2016; 2017; Le Moal et al., 2019).

48 Nutrients dynamics are governed by biological, chemical and physical processes and their interactions. Assimilation by
49 primary producers is a major biological factor regulating N and P concentrations in the aquatic environment. Aquatic micro-
50 and macro-organisms assimilate P as PO_4 and N mainly in fixed forms such as nitrate (NO_3) and ammonium (NH_4), but for
51 some specific organisms also in the form of N_2 . In estuaries, NH_4 is the preferred N-form ~~forby~~ microbes ~~in some cases like~~
52 ~~in estuaries~~ (Middelburg and Nieuwenhuize, 2000), but the uptake rate for both NH_4 and NO_3 can achieve maximum rates
53 under sustained exposure of NH_4 or NO_3 (Bunch and Bernot, 2012). Moreover, the nitrogen species are also involved in redox
54 transformations (Soetaert and Herman, 1995). Under anaerobic conditions, NO_3 can be reduced to NH_4 , in particular with high
55 organic matter contents, ~~or~~ It may also be denitrified to N_2 and N_2O . under such condition (Mulder et al., 1995), the latter is a
56 climate-active gas. Under aerobic conditions, NH_4 can be oxidized to NO_3 through nitrification by nitrifying microbes, which
57 is an O_2 consuming and acid generating process. Nitrification even occurs under cold conditions (below 10 °C) (Painter, 1970;
58 Wilczak et al., 1996; Cavaliere and Baulch, 2019).

59 The mixing of water from different flow routes is an important hydrological process that controls nutrient dynamics
60 (Rozemeijer and Broers, 2007; Rozemeijer et al., 2010a; Van der Grift et al., 2014; Yu et al., 2019). As nutrient concentrations
61 and speciation differ among different flow routes (Wriedt et al., 2007; Rozemeijer et al., 2010a; Yu et al., 2019; Yang and
62 Toor, 2019), the mixing process results in dilution or enrichment of nutrients in surface water bodies during precipitation
63 events (Wang et al., 2016).

64 Retention is another factor that determines nutrient concentrations and transport (McGlathery et al., 2001; Zhu et al., 2004;
65 Henry and Fisher, 2003), especially for phosphorus most of which is retained in inland water bodies sediment (Audet et al.,
66 2019). The retained P are either being permanently buried in the sediment or temporarily stored and acting later on as internal
67 nutrient source (Kleeberg et al., 2007; Filippelli, 2008; Zhang et al., 2018). Multiple researchers have highlighted the influence
68 of iron chemistry on the dynamics of P in pH neutral environments (Chen et al., 2018; Van der Grift et al., 2018). This is
69 especially relevant when iron-rich groundwater interacts with surface water (Griffioen, 2006; Rozemeijer et al., 2010a; Van
70 der Grift, 2014; Yu et al., 2019), in which P is immobilized by the formation of iron(oxy)hydroxides during groundwater
71 aeration. However, changes in chemistry or temperature may lead to the release of P and reduced iron. For instance, under
72 anaerobic conditions, Fe and P can be mobilized by sulfate reduction, but this can be counteracted by the presence of NO_3 as
73 electron acceptor (Smolders et al., 2006).

74 Most studies of eutrophication are based on discrete sampling events which can give a general pattern of nutrient dynamics,
75 but can easily miss important nutrient transport and processing phenomena (Rozemeijer et al., 2010; Rode et al., 2016; Toor
76 et al., 2017). The countermeasures to control eutrophication have been hampered because of limited knowledge of N and P
77 dynamics, for instance their response to changing weather conditions and land use (van Geer et al., 2016). In the past few years,
78 the development of new sensors and sampling technologies allow us to obtain data with substantially shorter intervals. In this
79 paper, the high frequency monitoring technology is referred to as an automatic monitoring program with sampling and
80 analyzing frequencies that are sufficient for obtaining detailed water quality variation information. High frequency technology
81 has proved to be a way to understand nutrient dynamics (Rode et al., 2016; Van Geer et al., 2016; Bieroza et al., 2018). Due
82 to the abundant information offered by this technology, combined methodologies have been developed to quantitatively
83 understand the in stream hydrochemistry of nutrients (Miller et al., 2016, Van der Grift et al., 2016, Duncan et al., 2017).

84 In our previous study on the water quality of Amsterdam (Yu et al, 2019), the transport routes of N and P from groundwater
 85 to surface water through seepage and drains were identified. In addition, spatial and temporal concentration patterns from
 86 discrete sampling campaigns showed a clear dilution pattern of other water quality parameters such as EC. However, the
 87 temporal patterns of N and P were still poorly understood, probably due to their reactive nature and more complex
 88 biogeochemistry. In order to obtain insight into the controlling mechanisms of N and P transport and fate in urban delta
 89 catchments affected by groundwater, we performed a year-round high-resolution N and P concentration monitoring campaign.
 90 A deep understanding of the water quality dynamic drivers would be a great asset for controlling eutrophication and improving
 91 aquatic ecological status (Fletcher et al., 2015; Díaz et al., 2016; Eggimann et al., 2017; Nizzoli et al., 2020). We conducted a
 92 one-year high frequency monitoring campaign in 2016-2017. Measured parameters were EC, NH₄, TP, turbidity and water
 93 temperature. The temporal patterns of these parameters were studied at three time scales: the annual scale, rain event scale,
 94 and pumping event scale.

95 2 Methods

96 2.1 Study site

97 The Geuzenveld study site is part of an urban lowland polder catchment, which is characterized by groundwater seepage that
 98 constantly determines the surface water quality, being the main source of solutes in the water system. The groundwater seepage
 99 is a continuous source of slightly brackish, anoxic, and iron and nutrient rich slightly brackish waters. Yu et al. (2019) presented
 100 the results of a 10 year monitoring program describing the main processes determining the water quality in the catchments,
 101 which is dominated by mixing of runoff water and seepage water. A high-frequency monitoring campaign was set-up to further
 102 unravel the temporal patterns of the nutrient N and P, of which N is typically present in the form of NH₄ from groundwater.
 103 Geuzenveld is a newly built urban polder on the west of the city of Amsterdam (Fig.1). Since the 1990s, when it was converted
 104 from agricultural to urban land, it has developed into a highly paved area. Similar to other new neighborhoods, Geuzenveld is
 105 equipped with a separated drainage system. A rain harvesting system was installed on all the buildings and houses in the polder,
 106 leading rain water from the roof and the street directly to the ditches, which results in fast and large amounts of runoff during
 107 storm events. Geuzenveld is a groundwater fed catchment due to the constantly higher groundwater head (-2.5 ~ -3 m NAP,
 108 NAP: Normalized Amsterdam Peil) in the main aquifer relative to the surface water level in the polder ditches (~ -4.25 m
 109 NAP)- (Fig.2). To keep the foundations of the building dry, there is a groundwater drainage system placed under an artificial
 110 sandy layer, right on top of a natural clay layer. The drain elevations range from -4.84 to -4.61 m NAP , which is below the
 111 phreatic groundwater level throughout the year, making sure that groundwater seepage either discharges through the drains or
 112 the ditches.

113 The water system of Geuzenveld is connected to the secondary water channel to its east, then connected to the adjacent primary
 114 channel, called boezem, the Boezem Haarlemmerweg. The boezem water level is -2.10 m NAP. It is much higher than the
 115 target surface water level of Geuzenveld, -4.25 m NAP. The surface water level in polder Geuzenveld is controlled by a pump
 116 station, which is the main outlet of this polder, situated in the northeastern corner.

117 There are two pumps (Pump 1 and Pump 2) in the pumping station, and they have different start and end pumping threshold
 118 points (Table 1).

119 **Table 1 Pumping scheme of polder Geuzenveld**

Time	Settings	Pump 1	Pump 2
05:00:00-19:00:00	Start point (m NAP)	-4.20	-4.16
	End point (m NAP)	-4.26	-4.24
19:00:00-05:00:00	Start point (m NAP)	-4.23	-4.18

End point (m NAP)

-4.31

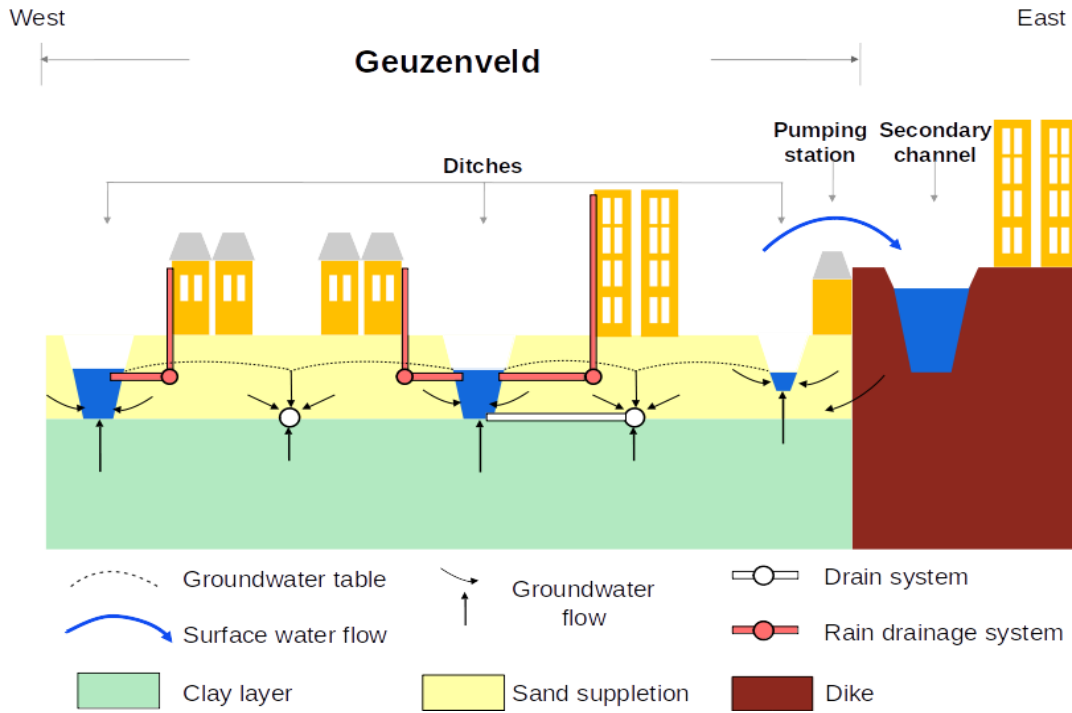
-4.29

120

121

The two pumps are activated when the surface water level exceeds the triggering level which are furthermore separated as day and night triggering levels (Table 1). The capacity of each pump is 3.6 m³ per minute. Most of the time, only one of the two pumps works and the surface water level is maintained between -4.31 m NAP and -4.23 m NAP, which are the night inactive and active pumping levels respectively. Normally, the surface water level drops immediately when the pump(s) start(s) working. Once the pump(s) stop(s), the surface water level will steadily rise due to the continuous inflow of groundwater seepage. During rainfall events, the surface water level rises faster (Fig.2A).

127



128



129

130 **Figure 1 Location of polder Geuzenveld (source: © Google Maps) and its landscape cross section and rain water and**
131 **groundwater drainage system**

132 2.2 Monitoring network setup

133 2.2.1 High frequency monitoring

134 A high frequency monitoring network was built on a temporary floating platform in front of the pumping station. The water
135 flowed around and underneath this platform to the pumping station when the pumps started working. One year time series of
136 $\text{NH}_4\text{-N}$ (mg L^{-1}), TP (and ortho-P) (mg L^{-1}), turbidity (Formazin Nephelometric Unit, FNU), electrical conductivity (EC, $\mu\text{S/cm}$)
137 and water temperature ($^{\circ}\text{C}$) were collected by the following equipment: a Sigmatax sampler combined with a Phosphax sigma
138 auto analyser for total phosphorus (TP), Amtax for $\text{NH}_4\text{-N}$ combined with a Filtrax automatic sampler, a Solitax-tline sc for
139 turbidity (manufactured by: Hach Lange GmbH Düsseldorf, Germany), and CTD-Diver for electrical conductivity (EC) and
140 water temperature (manufactured by: Van Essen Instruments, Delft, The Netherlands). The monitoring frequencies were set
141 to 20 mins, 10 mins, 5 mins, 5 mins and 5 mins interval for TP, $\text{NH}_4\text{-N}$, turbidity, EC and water temperature, respectively.

142 The Phosphax sigma is an analogue analyser for the high precision determination of total phosphorus concentration in
143 accordance with EN 1189 Phosphormolybdenum Blue method. Samples are automatically taken through a Sigmatax sampling
144 probe and include suspended solids. Subsequently, the sample is ultrasonic homogenized before delivery to the Phosphax
145 sigma. It is digested by the sulphuric acid-persulphate method (APHA/WWA-WPCF, 1989), and analysed with a LED
146 photometer (at 880 nm) (Hach, user manual of Phosphax sigma, 2016).

147 Samples for NH_4 are prepared by a filtration system, Filtrax. It continuously extracts samples through two ultra-filtration
148 membranes ($0.15 \mu\text{m}$) plates. Particles get dispersed by a continuous aeration system near the surface of the membranes (The
149 aeration caused severe build-up iron precipitants on the plates). The samples are then delivered to Amtax sc for analysis. The
150 ammonium in the sample is first converted to gaseous ammonia. Only the NH_3 gas passes through the gas-permeable membrane
151 of the electrode and is detected. This method guarantees a wide measuring range and is less sensitive to other compounds
152 compared to methods that make use of an ion-selective electrode (ISE). The Amtax sc in our study was calibrated automatically
153 at 22:00 every 24 hours before September 2016, every 48 hours thereafter. Maintenance work was conducted weekly as the
154 tubes were easily blocked by iron precipitates (Hach, user manual of Amtax sc, 2013).

155 The Solitax-tline sc sensor is a turbidity sensor with dual-beam optics and added backscatter. The measuring principle is based
156 on a combined infrared absorption scattered light technique that measures the lowest turbidity values in accordance with DIN
157 EN 27027 just as precisely and continuously as high sludge contents. Using this method, the light scattered sideways by the
158 turbidity particles is measured over an angle of 90° (Hach, User manual of Solitax sc, 2009).

159 The monitoring period of NH_4 and turbidity is from 2016-05-10 to 2017-06-16. Time series of phosphorus were obtained from
160 2016-05-23 to 2017-06-16. Electrical conductivity and temperature data are from 2016-06-10 to 2017-06-15. The NO_3 analyser,
161 Nitratax, time series consistently showed an artificial drift and proved to be unreliable in our field setting, possibly due to
162 biofilm accumulation in combination with iron oxides precipitation (see discussion). All the equipment outputs were integrated
163 into one wireless station. The monitoring station was shut down several times by lightning, so an electricity restart program
164 was also applied in this network. It worked for all equipment except for the Phosphax, which had to be restarted manually after
165 a black out.

166 Precipitation (hourly) and Evapotranspiration (daily) data were downloaded from the Schiphol KNMI station which is about
167 2 km away from Geuzenveld. Hourly pumping activity and surface water level data were obtained from Waternet, the water
168 authority of Amsterdam.

169 2.2.2 Low frequency monitoring

170 Since 2006, Waternet has monitored the water quality with a frequency of 12 times per year by sampling at the pumping station
171 of Geuzenveld. Between 2016 and 2017, the sampling frequency was increased to twice per month. We selected the following
172 parameters from the routine monitoring campaign: (1) EC, NH₄-N and TP to fill in the gaps in the continuous time series, and
173 to verify and monitor the potential drift and offset of the high frequency data and (2) pH, O₂, HCO₃, NO₃, TN, Kjeldahl-N,
174 suspended solids (detail of methods are described by Yu et al, 2019), chlorophyll-a, and transparency for further understanding
175 the biogeochemical processes. Organic-N was estimated by subtracting NH₄-N from Kjeldahl-N.

176 Bi-weekly total iron in the water column was analysed separately using ICP-AES (inductively coupled plasma-atomic emission
177 spectrometry). Total Fe was analysed from samples to which HgCl₂ was added for preservation and that were stored in a dark
178 and cool environment. To release all Fe that may have sorbed or precipitated during storage, we added 1 or 0.5 ml HCl in the
179 water samples to dissolve eventual flocks. Then the samples were homogenized in an ultrasonic bath for 24h, mixed again to
180 break down all the flocks. For extraction of all the Fe, we transferred 10 mL of the homogenized sample into a Teflon bottle,
181 added 3.2 mL HCl : HNO₃ 3:1 , and stored in a stove at 90 °C for 24 hours. The final solutions were analysed by ICP-AES.
182 Blanks were included and treated identical to samples.

183 2.3 Data processing and analysis

184 A correlation analysis between the high frequency and discrete monitoring data was applied to illustrate the reliability of the
185 high frequency time series. Furthermore, the time series data were analysed at 3 time scales: annual scale, rainfall events
186 (several days) and single pumping events (several hours). The relationships among the monitored parameters was explored by
187 testing their correlations at each time scale. At the annual scale, a correlation analysis was applied to the complete time period
188 and the wet and dry periods (definition in section 3.1.1). To discern the hydrological and chemical/biological attributes to the
189 observed dynamics, a linear mixing model was introduced at the annual scale, assuming precipitation and groundwater seepage
190 are the only water inputs, pumping and evapotranspiration are the only outputs, and pumping activity is the only way solutes
191 leave the water system. In this model, we assumed a constant seepage rate. Accordingly, surface water level was calculated
192 from:

$$194 \frac{dV}{dt} = (P(t) + S - E(t)) * A_{polder} - Pump(t) \quad (1)$$

$$195 L(t) = V(t)/A_{ditch} \quad (2)$$

196
197 V is total water volume in the ditches, P is precipitation, S is a constant seepage, E is potential evapotranspiration, A_{polder} is
198 area of the polder, $Pump(t)$ is water volume being pumped out with maximum capacity 216 m³ h⁻¹, A_{ditch} the area of the ditches
199 in the polder. L is surface water level in the ditches. Water level L determines the activation of pumping activity. Once $L(t)$
200 exceeds the upper ranges of water level (start point, section 2.1), the pumps will start to pump until L goes below the stopping
201 end (section 2.1) in the pumping scheme. Given the year-round seepage conditions throughout the polder, combined with an
202 artificially drained subsurface, we assumed that the potential evapotranspiration was close to the actual evapotranspiration
203 as no water shortages occur in our situation. In this study, we used the difference between groundwater head in the first
204 aquifer and the surface water level (Figure 2A) to estimate a range of the seepage. The actual number of 2 mm per day was
205 chosen based on the behavior of the mixing model and calibrated using the measured surface water levels (Figure S1).

206 A complete mixing of solutes was assumed in the model, which means that seepage, ditch water and precipitation mix
207 instantaneously when they enter the surface water. A delay from precipitation to run-off/drainage and to ditches was not
208 specifically considered.

209

$$\frac{d(VC)}{dt} = S * A_{polder} * C_{gw} + P(t) * A_{polder} * C_p - Pump(t) * C(t) \quad (3)$$

211

212 V is the ditch water volume given by equation (1), $C(t)$ is solute concentration at time t , C_{gw} is the average groundwater
213 concentration, C_p is the average concentration in runoff.

214 In our study area, the EC is a useful water quality parameter for describing the mixing processes between groundwater and
215 runoff water, as the EC represents the end members of the mixing: groundwater with an high EC (1750 $\mu\text{S}/\text{cm}$) and runoff
216 water (100 $\mu\text{S}/\text{cm}$) with a low EC (see also Yu et al., 2019). Moreover, we assume that EC behaving as a conservative tracer
217 as the EC is highly correlated with the Cl concentration ($R^2 = 0.71$, p -value < 0.05) and the temporal patterns of EC and Cl are
218 very similar (see supplement Figure S2). In the model, seepage rate was adapted to get the best fit between the modeled and
219 the measured EC. The calibrated seepage rate was 2.0 mm d^{-1} . Compared to EC, nutrients are highly reactive solutes and thus
220 can vary a lot along their flow routes due to biogeochemical processes. The model provided a tool to simulate concentration
221 dynamics under the assumption that EC, NH_4 and TP were conservative. The simulated concentrations of EC, NH_4 -N and TP
222 were plotted together with the high frequency measured time series. A comparison between the modeled and the measured
223 results was performed by using correlation analysis.

224 The average concentration of EC in groundwater was set equal to the average of the sampling survey, which was 1750 $\mu\text{S}/\text{cm}$
225 (including both deep and shallow groundwater, Yu et al., 2019). For the NH_4 and TP concentration data, we chose the
226 measurement from a drain sampling point (Drain 3, Yu et al., 2019) in the middle of the polder as the non-disturbed
227 groundwater collected by the drains in this area of the polder. They were 8.1 mg N L^{-1} and 1.6 mg L^{-1} respectively. The starting
228 (01-06-2015) concentrations were 1200 $\mu\text{S}/\text{cm}$, 4 mg L^{-1} , and 2 mg L^{-1} for EC, NH_4 , and TP respectively. The model was not
229 sensitive to the selected end-member values.

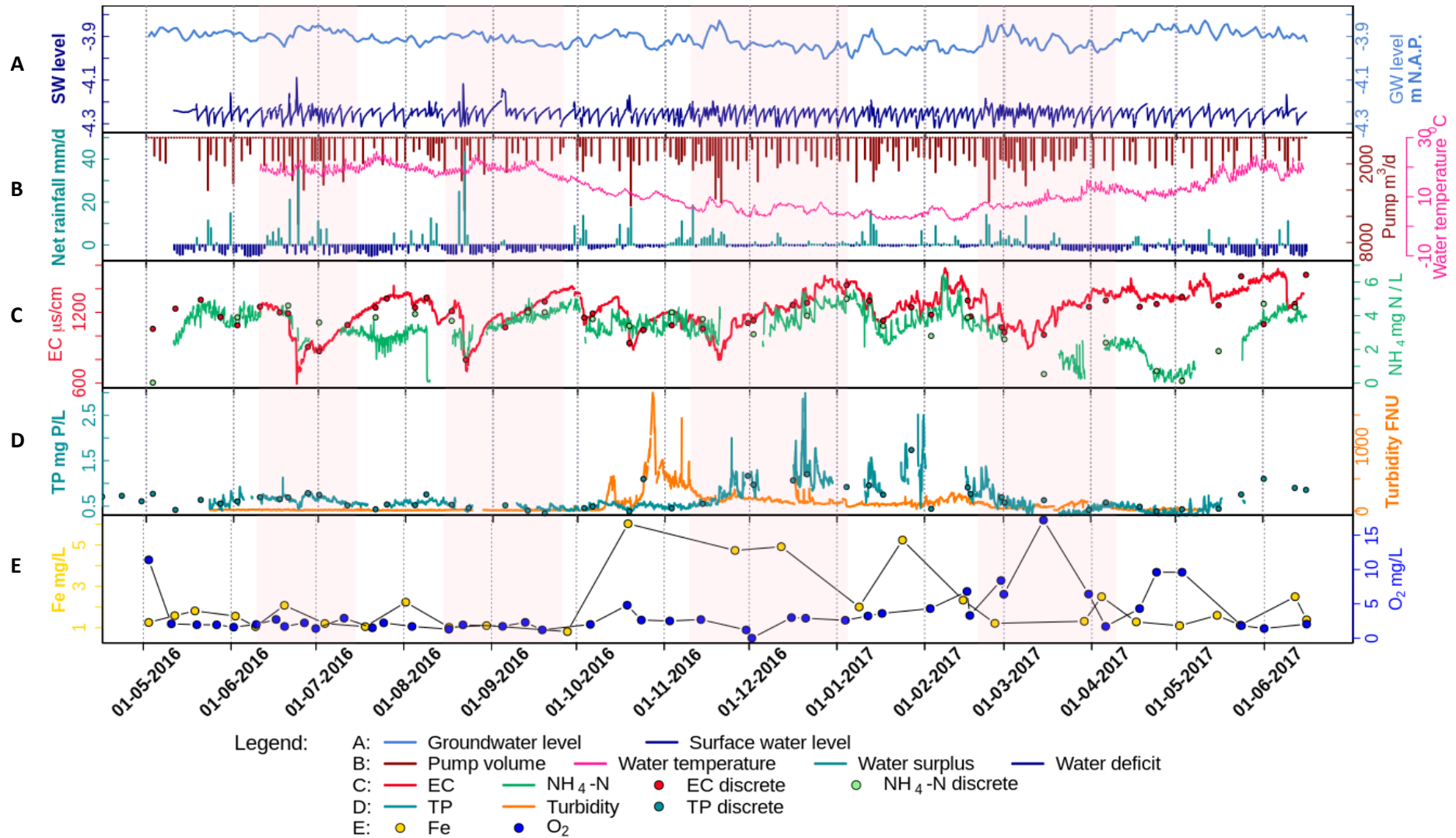
230 The time series data were further analysed at shorter scales: rain event scale and pumping event scale. Four rain events were
231 selected according to the dilution extent of EC, defined as an EC value reduced by over 35%, they were: 10-06-2016 ~ 15-07-
232 2016, 15-08-2016 ~ 26-09-2016, 10-11-2016 ~ 05-01-2017, and 20-02-2017 ~ 10-04-2017. These four events covered both
233 EC dilution during rainfall and the recovery afterwards in different seasons. We selected 4 representative pumping events to
234 present the response of EC, NH_4 , TP, and turbidity to the pumping activities. Those events were in 15-07-2016 ~ 17-07-2016,
235 27-10-2016 ~ 29-10-2016, 20-12-2016 ~ 22-12-2016, and 05-05-2017 ~ 07-05-2017. Correlation analysis was as well applied
236 to each event at the corresponding two time scales, averaging over whole days for precipitation events and over hours for
237 pumping events. Data processing and analyzing were performed using Rstudio (R version 4.0.2) and time series package "xts".

238 3. Results

239 3.1 Annual pattern of meteorological, hydrological, and water quality time series

240 3.1.1 Meteorological and hydrological conditions in polder Geuzenveld

241 To explain the time series (Fig. 2), we distinguish between dry/wet periods and dry/wet seasons. The wet and dry periods (days
242 to weeks) are represented by a water surplus (light blue color in Fig.2B, daily evapotranspiration $<$ daily precipitation) or a
243 water deficiency (dark blue in Fig.2B, daily evapotranspiration $>$ daily precipitation). We defined the wet and dry seasons
244 based on water surplus and deficit. The average net rainfall (the water surplus/deficit in Figure 2) is 1.4 mm/d for the period
245 of 01-10-2016~15-03-2017, and -0.8 mm/d for the rest. Subsequently, we statistically analysed the difference between these
246 two periods for multiple parameters. Table 2 shows the mean of each parameter for the wet and dry seasons and their
247 significance test results. The wet and dry seasons means are significant^{ly} different for all parameters, but the EC.



248
 249 **Figure 2** Time series of (A) surface water level (SW level) and groundwater level (m NAP), (B) net rainfall (daily water surplus (+) (lightblue) and deficit (-) (darkblue), mm d⁻¹)
 250 and daily pumping volume (Pump m³ d⁻¹), (C) hourly time series of EC (µS/cm) and NH₄-N (mg N L⁻¹), and (D) hourly TP, turbidity, (E) discrete samples of Fe (total iron in
 251 water column) and O₂ concentrations (mg L⁻¹). The dots in (C) and (D) are the corresponding discrete sampling data, which are plotted to show their close match to the
 252 continuous time series data, as well as to fill in the gaps. All data were monitored at the pump station. The transparent pink blocks are the selected rain events for further
 253 analysis in section 3.3. [See Table S1-S3 for the correlation tests performed on the dataset.](#)

Table 2 The mean of each parameter, and the significance for the wet and dry seasons

	Net rainfall* mm/d	Pump volume* m ³ /d	Water temperature* °C	EC µs/cm	NH ₄ * mg N/L	TP * mg P/L	Turbidity* FNU	Fe* mg/L	O ₂ * mg/L
Wet	1.4	1050	6.7	1212	3.7	0.8	197	3.4	4.3
dry	-0.8	712	17	1252	3.0	0.5	15	1.5	3.3

* $p < 0.05$ ¹

255

256

257 Over the whole monitoring period, the water temperature ranged between 2 to 26 °C. From June to mid-September 2016, the
258 temperature remained above 18 °C, then declined to become lower than 10 °C at the end of October. The following four months
259 (November to February) were the coldest. Especially in January and February 2017, during which the water temperature
260 dropped to below 3 °C. By the end of February temperatures started to rise again to reach 10 °C by the end of March 2017.

261 The surface water level in Geuzenveld has been maintained between -4.31 and -4.1 m NAP, strictly regulated by pumping
262 (Fig.2A). After the pumps stopped, the surface water level recovered faster during the wet season (between October 2016 and
263 March 2017) than during the dry season. Similarly, the shallow groundwater level positively corresponded to the precipitation
264 and negatively to the daily accumulative pumping volume. The phreatic groundwater level in Fig.2A (light blue) was from
265 one of the piezometers, which lies right outside of the polder (Figure 1, 52°22'46.0"N 4°47'15.6"E). In contrast to the constant
266 surface water levels (Fig.2A, dark blue), the shallow groundwater had relatively low levels in the wet season compared to the
267 dry season. This is related to the water level regulation of the boezem Haarlemmerweg with higher levels in summer than in
268 winter (<https://www.rijnland.net/actueel/water-en-weer/waterpeil>). Phreatic water levels were consistently 20-40 cm higher
269 than the surface water level in the polder, which confirms the continuous groundwater seepage into the surface water system.

270 3.1.2 Annual water quality patterns

271 The ~~Pearson's coefficients of determination (R^2)~~ ~~coefficients of determination (R^2 "Pearson" method used)~~ between the high
272 frequency data and the routine discrete sampling data from the water authority are 0.88 for EC (p -value < 0.05), 0.92 for NH₄
273 (p -value < 0.05), and 0.97 for TP (p -value < 0.05). The scatter plots between the high and low frequency measurements are
274 shown in Figure S7.

275 During a rainfall event, rain and runoff from pavements and roofs, which were collected by a separate drainage system, directly
276 fed the surface water (Fig.1). Distinct rainfall events cause a strong dilution pattern of both EC and NH₄ (in Fig.2C). The EC
277 ranged from 600 to 1500 µS/cm. In general, during rainfall events, the EC declined because of dilution, while, after the events,
278 EC gradually rose back up to around 1500 µS/cm. The duration of this process, i.e. *recovery time*, was longer in the wet season
279 than in the dry season. A similar pattern of dilution and recovery is also visible for NH₄, especially for the period August 2016
280 – March 2017, where NH₄ shows a very similar response as EC (Table S2, wet season, $R^2 = 0.73$), although with somewhat
281 larger day to day fluctuations. However, a contrasting pattern without NH₄ recovery occurred twice: from the middle of June
282 to the end of August 2016 and from the middle of March to the middle of May 2017. During these periods, concentrations of
283 NH₄ were considerably lower and deviated from the slope of the EC pattern. NH₄ decreased from around 4 mg L⁻¹ to around
284 2 mg L⁻¹ between the middle of June to the end of August 2016, but the continuous NH₄ measurements are not supported by
285 the discrete samples which follow the EC pattern more closely. During the second period from March to the middle of May
286 the deviation from the recovery pattern is more pronounced, and NH₄ concentrations dropped to almost 0 mg L⁻¹ and started
287 recovering from the beginning of May. This pattern is fully supported by the available discrete samples. During the same

¹ Wilcoxon rank-sum test. The tests were performed in Rstudio (version 3.6.1), `wilcox.test()` in package "stats".

288 period in 2016 the high-frequency monitoring had not yet started, a single NH_4 discrete measurement is available for the 2nd
289 of May, that seems to reveal a similar pattern in the spring of 2016.

290 Both TP and turbidity showed contrasting patterns during the wet and dry seasons (Fig. 2D). Turbidity stayed below 60 FNU
291 during the dry season until October and rapidly increased after a first rain event to 500 FNU (more details refer to Figure S3
292 in supplementary information). A drop to about 200 FNU occurred right after this first peak, which seemed to correspond to
293 excessive precipitation and a large pumping volume (Fig.2B). Soon after, turbidity went up again and peaked at 1800 FNU.
294 Turbidity leveled off towards values around 200 FNU for the rest of the wet season and dropped below 60 FNU from April
295 2017 onwards.

296 TP concentrations were significantly higher during the period between 15-11-2016 and 01-03-2017 than the rest of the time
297 (p -value < 0.001, Figure S5), during which TP fluctuated around 0.5 mg L^{-1} , but always below 1 mg L^{-1} . During the wet season
298 with the low temperatures (Table S2, $R^2 = -0.68$), TP almost constantly stayed above 1 mg L^{-1} and even reached values of
299 about 3 mg L^{-1} in December. Although there were large gaps in the TP time series during this period, the high TP concentrations
300 appear to have been diluted by rain events, for example the event at around January 10th, 2017. Most discrete samples
301 measurements of TP matched well with values from the high frequency time series (Fig.2D, Table S1, $R^2 = 0.88$).

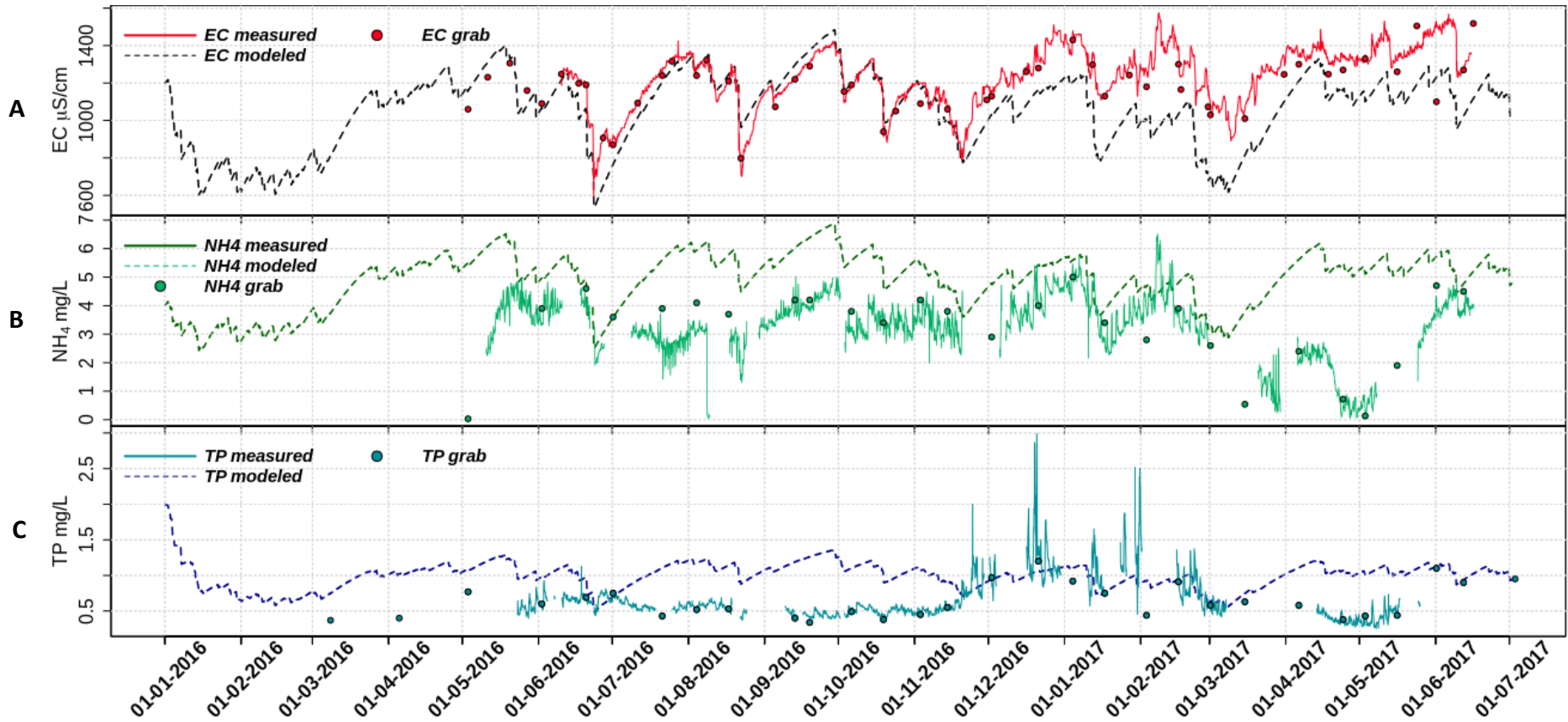
302 Total-Fe concentrations were most of time lower than 2 mg L^{-1} (Fig. 2E), but for the wet season concentrations were higher
303 and reached up to about 6 mg L^{-1} . The initiation of Fe increases at the beginning of the wet season coincided with that of
304 turbidity (Fig.2D and Table S2, $R^2 = 0.72$). Upon the increasing temperature in March 2017, total Fe concentrations dropped
305 back to below 2 mg L^{-1} (a negative correlation between temperature and Fe is shown in Table S1). Dissolved O_2 concentrations
306 were generally low in the water column; i.e. usually below 5 mg L^{-1} . Concentrations of over 3 mg L^{-1} were only found in
307 March, April and May.

308 3.2 Model of water quality time series based on water balance

309 A simple fixed-end-member mixing model was used to reconstruct the conservative mixing of EC, NH_4 , and TP. The simulated
310 and the measured EC, NH_4 , and TP are plotted in Figure 3. The correlations between the modeled and measured results are
311 shown in the supplementary information (Table S4-S6). Potential processes that might deprive or enrich nutrients relative to
312 the conservative mixing process along the flow routes were inferred from the discrepancies between the modeled and the
313 measured data. Figure 3(A) and Table S5 show that the predicted and observed EC dynamics agree reasonably well from May
314 to November 20th, 2016 ($R^2 = 0.91$). After that, the conservative mixing approach underestimated the EC but the main dynamics
315 and the amplitudes were still reproduced (Table S6, $R^2 = 0.82$); as groundwater is the only contributor to the high EC due to
316 the seepage of quite mineralized, slightly brackish water, the model must underestimate the seepage flux from November 20th,
317 2016 on. Overall, the observed dynamics of EC are consistent with mixing of high EC seepage water with low EC runoff water
318 (coefficient of determination between the modeled and measured EC is 0.65 over the complete period, Table S4).

319 The dynamics of measured NH_4 concentrations show close resemblance to the model results, especially during the wet season
320 (01-10-2016~15-03-2017). Clearly, NH_4 is diluted during the rain events and a gradual increase of NH_4 starts after each rain
321 event during the wet season showing slopes that resemble the model reconstruction. Over the whole period, measured NH_4
322 concentrations were overestimated by the model, indicating that some NH_4 is probably lost due to non-conservative processes.
323 This is especially true for the spring season of 2017, where NH_4 concentrations must be controlled by additional processes.
324 Concentrations of TP are generally far below the conservative model reconstruction, except between the end of November and
325 the beginning of March. During this particular period the minimum measured TP concentrations are captured nicely by the
326 conservative model, ~~however-but the~~ distinct peaks up to 3 mg L^{-1} ~~are not are not captured by the model and must have different~~
327 ~~physical or chemical processes determining them.~~

328



329
 330
 331
 332
 333

Figure 3 Plots of fixed-end-member mixing model predicted (A) EC, (B) NH_4 and (C) TP with their measured time series data and the discrete sampling results. [See Table S4-S6 for the correlation tests performed on the dataset.](#)

334 3.3 Water quality responses to single events analysis

335 To elucidate the response pattern of water quality to precipitation and pumping activity, we selected four major events (Fig.2
336 (4 pink shades) and Figure 4) and four pumping events (Figure 5). The former events were chosen according to their clear
337 dilution pattern of EC (Fig.4), while the latter were pumping events without occurrence of rainfall (Fig.5). All seasons were
338 covered, including some of the wet and dry periods.

339 3.3.1 Rainfall events

340 EC and NH_4 showed clear dilution and recovery patterns during all events, while the pattern was not clear for TP and turbidity
341 (Fig.4). The extent of dilution of EC appears to depend on the precipitation intensity. Rainfall during the recovery period
342 determined how long it took to recover back to the highest level. The short but intensive rainfall during dry season events 1
343 and 2 reduced EC rapidly from around 1300 to around 700 $\mu\text{S}/\text{cm}$, while the recovery took about 1 month. Events 3 and 4 had
344 less rainfall and dilution of EC was less (from about 1300 to about 800 $\mu\text{S}/\text{cm}$) and recovery took more than one and a half
345 month in event 3, during which multiple small events occurred. The dilution patterns of the NH_4 in events 1 and 2 were similar
346 to those of EC ($R^2 = 0.86$ and 0.83 , respectively, Table S7 & S8) and show resemblance for event 3 ($R^2 = 0.75$, Table S10).
347 Moreover, a direct negative correlation between NH_4 and rain intensity supports this dilution effect for event 2. Due to the data
348 gaps of NH_4 in event 4 we cannot completely describe the pattern of NH_4 for this one, but it corresponds with that start of
349 reduced NH_4 which was described in sections 3.1 and 3.2.

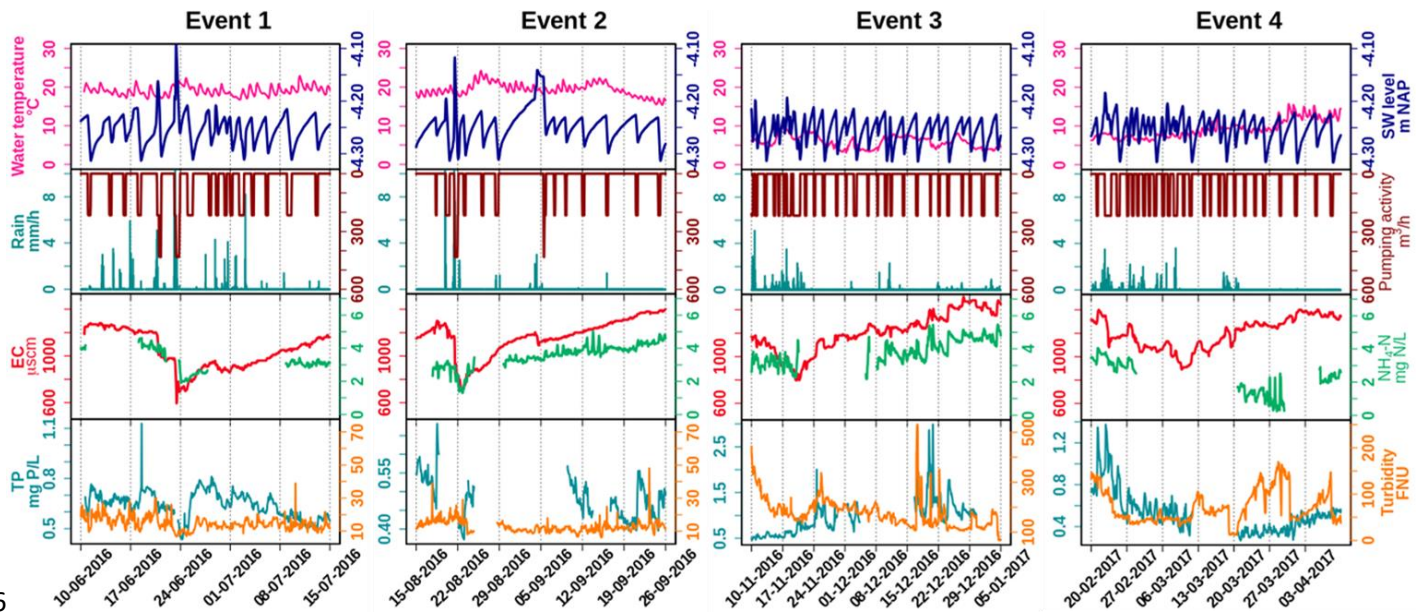
350 The response of TP was generally not related to the intensity of rainfall and pumping, except for event 3 during the wet period.
351 Dilution effects, as were observed for NH_4 , were not observed for TP for events 1, 2 and 4. During the wet season event 3, TP
352 concentrations show negative correlations with precipitation and pumping intensity ($R^2 = -0.79$ and -0.59 , respectively, Table
353 S9) and correspond with decreasing turbidity. Event 4 marks the transition between the wet and dry season and the drop in TP
354 coincides with the drop in NH_4 , independently from individual rain storms during the dry season.

355 During the dry season (with event 1 and 2 included) turbidity always stayed below 50 FNU. Turbidity sometimes showed
356 single peaks which are likely related to disturbances of the floating platform by wind and should probably be treated as false
357 signals. Turbidity is more variable and has higher variance for wet season events 3 and 4, which corresponds with the findings
358 of the annual scale analysis (section 3.1.2). During event 3, turbidity varied between 100 and 500 FNU. Although clear relations
359 exist between Fe, TP and turbidity, all higher during the wet season (Figure 2, Table S2), these are not clearly reflected at the
360 scale of individual precipitation events. Simultaneous peaks of TP and turbidity occur that are not easily related to the weather
361 conditions in November and December but TP and turbidity show contrasting signals at the start of the event. The turbidity
362 clearly decreases during rain storm event 3 and at the start of event 4. This change is not reflected by the correlation at the total
363 event scale (Tables S9 and S10) but obvious when studying only the time scale of the decreasing limb of the EC dilution.
364 Event 4 coincides with the transition to the spring season in 2017, showing decreasing EC, TP and turbidity in the last rains of
365 the wet season and a strong decrease of NH_4 and increase of turbidity when conditions dried up and temperatures rose.

366 3.3.2 Pumping events and day and night pattern

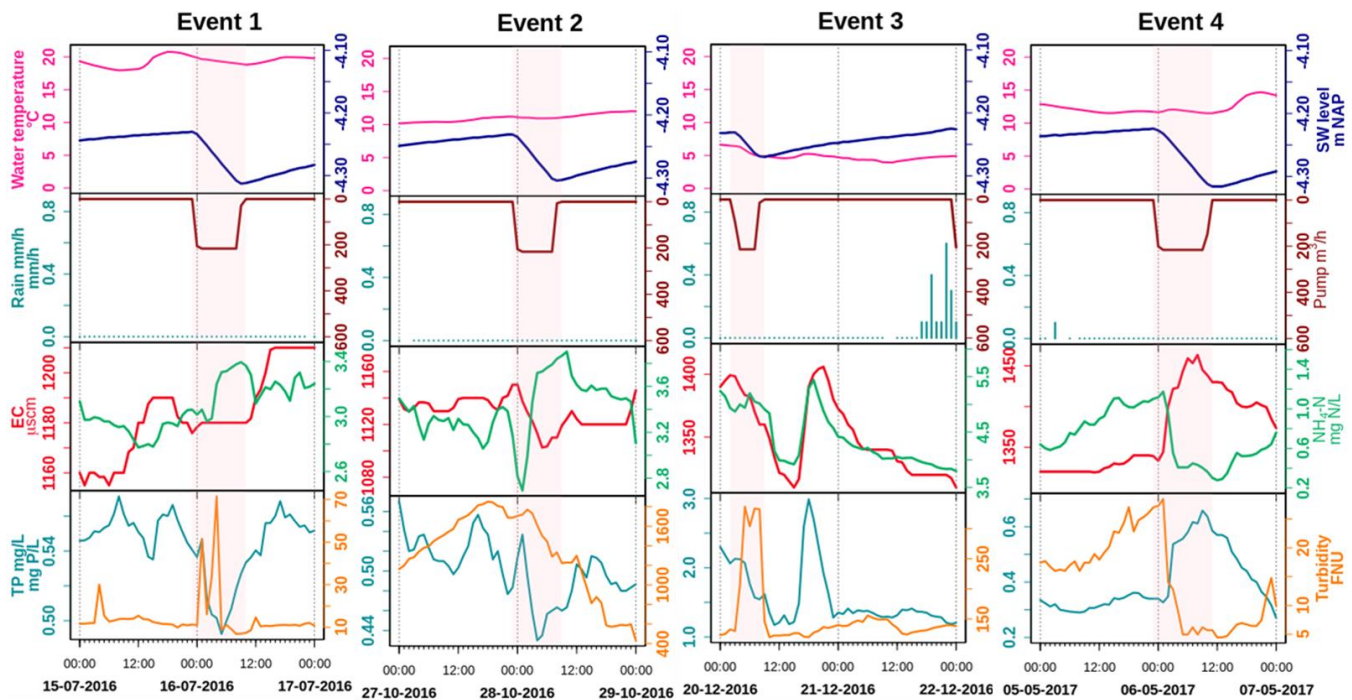
367 The selected pumping events covered four seasons: summer (2016 July, event 1), autumn (2016 October, late autumn, event
368 2), winter (2016 December, event 3) and spring (2017 May, event 4) (Fig.5). While the effects of pumping on EC are rather
369 small, TP, NH_4 and turbidity are all affected by pumping. The effects of pumping appear to be different for events in different
370 seasons; turbidity for example increases during pumping in July and December but decreases in May. The increase during the
371 December pumping is especially marked (R^2 Pumping intensity versus Turbidity = 0.77 , Table S13). TP decreases during
372 pumping in July ($R^2 = -0.67$) and October and increases in May ($R^2 = 0.6$). Event 2 seems to have started a major drop in
373 turbidity (more than 1000 FNU) that continued some time after pumping.

374



376

377 **Figure 4** Selected events showing dilution and peaks of water quality parameters, with hourly precipitation (mm/h)
 378 and hourly pumping activity (m^3/h). Note that between events different scales of TP and turbidity were used to reveal
 379 the dynamics. [See Table S7-S10 for the correlation tests performed on the dataset.](#)
 380



381

382 **Figure 5** Pumping and pumping effect patterns on water quality, blue blocks represent the pumping duration. [See](#)
 383 [Table S11-S14 for the correlation tests performed on the dataset.](#)

384 4. Discussion

385 This study aimed at understanding the dynamics of N and P fluxes from the low-lying urban polder of Geuzenveld to
 386 downstream surface waters in order to eventually support water managers to mitigate eutrophication. Based on our high-
 387 resolution water quality measurements, we found that the surface-water chemistry at the polder outlet pumping station is
 388 governed by a complex combination of hydrological mixing and biogeochemical processing. In the following discussion, we
 389 start with [the presentation of](#) the relatively straightforward dilution behavior of EC, followed by adding the impact of primary

390 production (i.e. algae growth) for understanding the NH_4 concentration patterns, and benthic primary producer and iron
391 chemistry for understanding the turbidity and TP concentration patterns.

392 4.1 Hydrological mixing between groundwater and rainfall

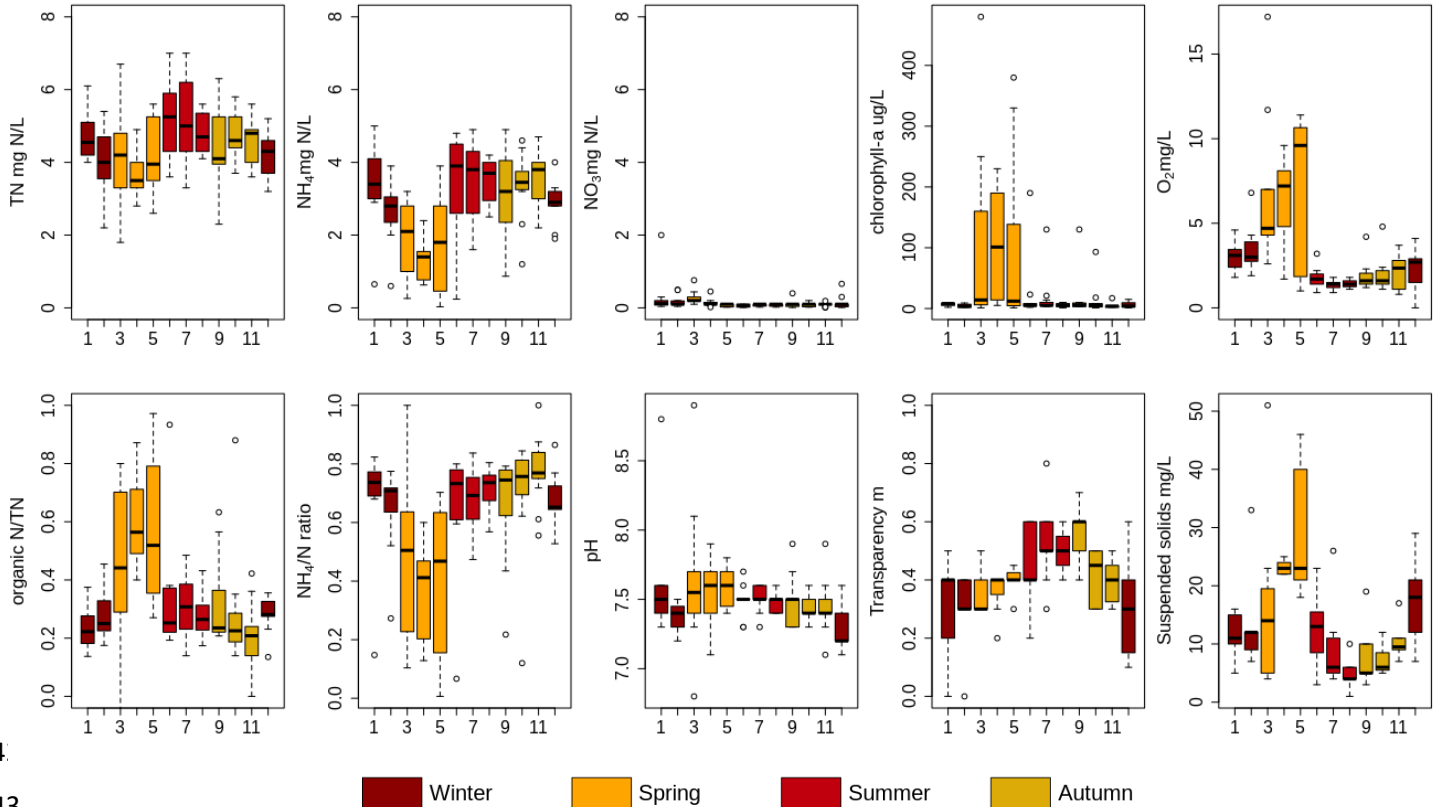
393 In a highly manipulated low-lying urban catchment like Geuzenveld, mixing between rainwater and groundwater in the ditches
394 is fast due to the high fraction of impervious area and the installation of both a rainwater and a groundwater drainage system
395 that transport these contrasting water types efficiently to the ditches (Yu et al., 2019; Walsh et al., 2005). Runoff in Geuzenveld
396 has EC of about $166 \mu\text{S}/\text{cm}$ (Yu et al., 2019), which is lower than the groundwater EC ($1746 \mu\text{S}/\text{cm}$ on average). As a relatively
397 conservative water quality parameter (Figure S2), mixing between rainwater and groundwater should be the main process for
398 EC. This presumption is supported by the agreement between the modelled and the measured EC dynamics for the period
399 between May to November 2016. Precipitation events diluted the EC values at the pumping station, and the magnitude of
400 dilution depended on the intensity of precipitation; heavy rainfall resulted in low EC values (Fig.2D and Fig.4). In periods
401 with the absence of rainfall, the EC values follow a recovery curve that resembles a linearly mixed reservoir with
402 concentrations increasing to values that approach the EC of the continuous groundwater supply of around $1500 \mu\text{S}/\text{cm}$. After
403 November 2016, ~~the conservative mixing approach underestimated the EC~~ was underestimated by the model, but the main
404 dynamics were still reproduced and the amplitude of the EC dynamics remains similar to the model results, except for the short
405 period Nov 20th to Dec 1st 2016. Starting around The sudden increase of the measured EC around Nov 20th, the EC started
406 to increase relative to the dry season before. It coincides with an intensive pumping event after the first intensive rainfall event
407 that happened after a prolonged period of cumulative water deficit. This may be related with a first flush from the drain system
408 that starts to be activated more strongly, thus removing clogged material and lowering the overall resistance of the drain system
409 for shallow and deep groundwater inflow (van der Velde et al., 2010). It suggests that this triggered the inflow of somewhat
410 more mineralized groundwater relative to the period before, creating a shift in the EC towards $\sim 250 \mu\text{S}/\text{cm}$ higher values that
411 continued during the remainder of the monitoring campaign. It appeared that it raised the EC, but did not change its the
412 amplitude or dynamics of the EC during the remainder of that period (Fig. 2 and 3, Table S6). The elevated EC may
413 alternatively due to the application of road salts in winter which starts from November. An alternative reason for the higher EC
414 starting from November, 2016 on, would be the application of road salts during the winter period. Although freezing conditions
415 occurred from November onwards, But we did not find any evidence for the prolonged effects of road salts, as the chloride
416 concentrations in the grab samples only showed two higher measurements, one in December 2016 and one in January 2017
417 (see Supplement, Figure S2). So, overall, the observed dynamics of EC are consistent with mixing of high EC seepage water
418 with low EC runoff water.

419 The mixing process can explain part of the dynamics of NH_4 and TP in the wet season, but insufficient for explaining the
420 dynamics during the dry season due to the presence of biological and chemical processes. During winter, mixing can also
421 explain the dynamics of NH_4 and TP (Fig.3). Compared with groundwater, which carries around $8 \text{ mg L}^{-1} \text{ NH}_4$ and 1.6 mg L^{-1}
422 TP , rain and runoff have much lower nutrient concentrations, which makes groundwater the main nutrients source (Yu et al.,
423 2019). Nutrients derived from groundwater mix with rainwater in the ditches through direct seepage and the efficient
424 groundwater drainage systems. Clearly, NH_4 is diluted during the rain events and a gradual increase of NH_4 starts after each
425 rain event during the wet season showing slopes that resemble the model reconstruction. Over the whole period, measured
426 NH_4 concentrations are The overestimated overestimation of the modeled NH_4 in general by the model, indicating that some
427 NH_4 is a probably lost to transformation processes. This is, especially true in the spring season of 2017, where NH_4
428 concentrations must be controlled by other processes. Concentrations of TP are also generally far below the conservative model
429 reconstruction, except between the end of November and the beginning of March. During this particular period the minimum
430 measured TP concentrations are captured nicely by the conservative model, however. The distinct peaks up to 3 mg L^{-1} are not
431 captured by the model and must have be determined by different physical or chemical processes determining them. While the

432 mixing process can explain part of the dynamics of NH_4 and TP in the wet season, the mixing assumption cannot explain the
 433 behavior of NH_4 and TP during other seasons, when NH_4 and TP measured time series drift far below from the conservative
 434 mixing model pattern because of biological and chemical processes.

435 4.2 Primary production and nutrients

436 NH_4 dynamics during winter can be explained by mixing. However, biological processes are overruling the mixing process
 437 during spring and summer. It resulted in lower measured NH_4 concentrations than modeled during this period. Studies have
 438 shown that benthic and planktonic primary producers (e.g. phytoplankton) assimilate nutrients and are an important factor
 439 controlling nutrient dynamics in rivers, lakes, and streams (Hansson, 1988; Jäger et al., 2017). In polder Geuzenveld, the
 440 biological nutrient uptake is not only reflected in the time series data (Fig.2 and 3, Table S3) but is also evident in the monthly
 441 measurements from the water authority for the period 2007-2018, as summarized in Figure 6 and Table S15-S19.



442
 443
 444 **Figure 6 Monthly measurements of TN, NH_4 -N, NO_3 -N, chlorophyll-a, O_2 organic N/ TN and NH_4 -N/TN (NH_4 /N)
 445 mass ratio, pH, water transparency, and suspended solids in Geuzenveld from 2007 to 2018. X axis is month. [See](#)
 446 [Table S15-S19 for the correlation tests performed on the dataset.](#)**

447
 448 The increasing availability of light (and temperature increase) during spring (Figure S6), induces growth of primary producers.
 449 Growth of primary producers results in consumption of ammonium, phosphate and a production of organic-N, chlorophyll-a,
 450 oxygen, and suspended solids, and led to a relatively higher pH because of the uptake of CO_2 (Figure 6, Table S16). These
 451 patterns are also clearly reflected in the shift in the NH_4 /TN and organic-N/TN ratios during spring (Figure 6). Primary
 452 production occurs both in the water column by phytoplankton as well as by benthic algae. Macrophytes could in principle also
 453 contribute, but they were absent in Geuzenveld. One of the structuring factors governing the relative importance of benthic
 454 and planktonic primary producers is light availability: benthic algae and macrophytes tend to dominate in shallow and clear
 455 waters, while phytoplankton is more likely to dominate in deeper and more turbid waters (Hartwig, 1978; Jäger and Borchardt,
 456 2018; Petranich et al., 2018; Middelburg, 2019). Although our data do not allow conclusive determination whether benthic or
 457 pelagic primary producers dominate, it appears that their relative importance varies with season.

458 These primary producers also compete for nutrients. Benthic primary producers have direct (macrophytes) or first (benthic
459 algae) access to nutrients that seep up from the subsurface, while planktonic primary producers depend on nutrient supply from
460 surface runoff and nutrients remaining after consumption by benthic primary producers. For example, Henry and Fisher (2003)
461 found that benthic algae can remove up to 80% of nitrogen from an upwelling water source. As we stated above, nutrient-rich
462 groundwater is the major source of N and P to surface waters in polder Geuzenveld. In addition, due to the shallow depth of
463 the ditches, light reaches the bottom with the consequence that benthic algae can proliferate in this polder. These benthic
464 primary producers might utilize the up-flowing nutrients from groundwater and intercept the nutrients from seeping further
465 into the water column (Hansson, 1988; Pasternak et al., 2009). The increasing light availability and thus primary production
466 during spring led to the nearly complete deprivation of NH_4 in the water column (Fig.2C).

467 Following the spring bloom, concentrations of chlorophyll-a (proxy for phytoplankton biomass) and O_2 dropped substantially,
468 while NH_4 concentrations rapidly recovered to around 4 mg L^{-1} in both the time series (Fig.2C) and the long-term monthly
469 sampling results (Fig.6). Dissolved O_2 remained low (close to hypoxia) during the whole summer (below 2 mg L^{-1}) (Fig.2E
470 and Fig.6), indicating that oxygen consumption by organic matter degradation and re-oxidation of reduced components from
471 groundwater seepage outcompeted oxygen production from primary production. During summer, suspended solid and
472 chlorophyll-a concentrations were low (Fig.6), indicating low biomass of plankton algae. Suspended solid and phytoplankton
473 dominate light attenuation (Scheffer, 1998; Middelburg, 2019). Consequently, during this period, we observed an abrupt shift
474 of the water regime from a turbid state to completely clear, as reflected in the high transparency from June to September (Fig.
475 6). The low biomass of phytoplankton might be due to N limitation as nutrients are intercepted by benthic algae at the sediment
476 interface. An alternative explanation is that zooplankton grazing maintained phytoplankton biomass low (Strayer et al., 2008;
477 Genkai-Kato et al., 2012).

478 Temperature and light reaching the sediment started to fall from September onwards (Figure S6), thereby reducing the intensity
479 of biological activity, including NH_4 assimilation. Consequently, NH_4 started to behave conservatively again like EC (Fig.2 &
480 Fig.3). The best fit between the modeled and measured NH_4 was from the end of November to the beginning of March, i.e.
481 during the winter period with lower light levels and shorter day lengths and very low primary production. The absence of
482 primary production during winter, leads to conservative behavior of NH_4 governed by the mixing between groundwater and
483 rain water.

484 485 **4.3 P binding and turbidity**

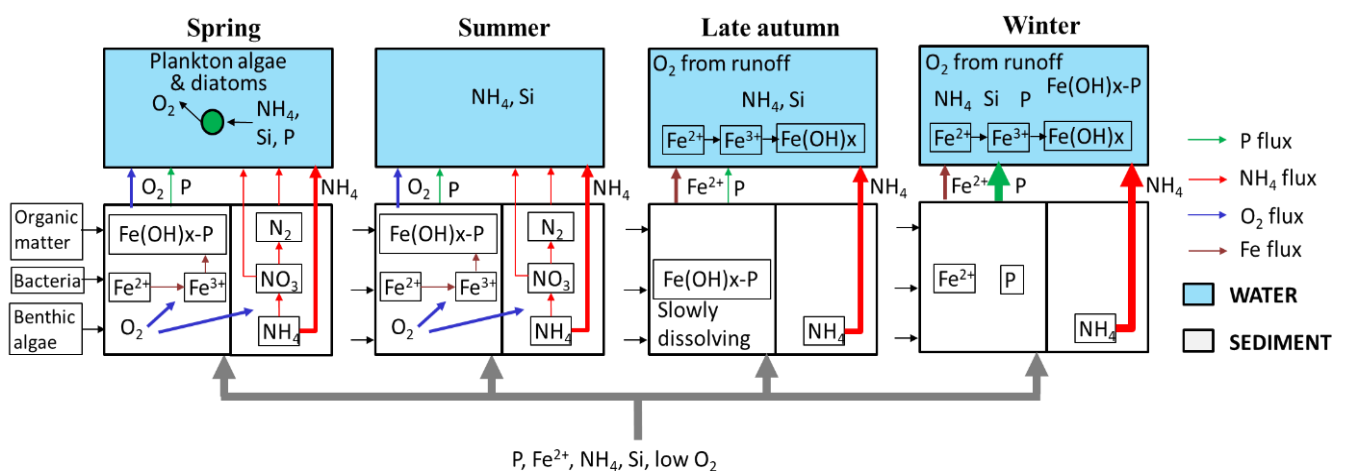
486 Iron chemistry is considered the dominant process governing the P dynamics in shallow groundwater fed ditches (Lijklema,
487 1994; Smolders et al., 2006; van der Grift et al., 2018). However, primary producers take up P for growth and at the same time
488 release O_2 that regulates iron chemistry in lake water column (Table S1-S3, Spear et al., 2007; Zhang and Mei, 2015; Lu et al.,
489 2016). This web of interactions likely controls P dynamics in these ditches.

490 From spring to autumn, TP concentrations were fluctuating around 0.5 mg L^{-1} , and the water had low turbidity ($<50 \text{ FNU}$),
491 thus high transparency allowing the growth of benthic algae that produce oxygen. Consequently, when P and Fe rich anoxic
492 groundwater reaches the surface water-sediment interface, Fe oxidized into iron hydroxides in a short time (Van der Grift et
493 al., 2014). P is then sorbed onto those Fe-hydroxides and retained in the sediments. Oxidation of reduced iron consumes O_2 ,
494 contributing to the low O_2 conditions of the water column (Fig.2E). Moreover, it leads to the formation of a reddish-brown
495 film of ferric iron (hydrated ferric oxide, Baken et al., 2013; van der Grift et al., 2018) on the bottom of the ditches, which can
496 be seen in summer when the water was transparent. This slimy layer comprising iron hydroxides and benthic microbes can
497 easily be resuspended and therefore act as a source of turbidity following perturbations by pumping, wind, rain or foraging
498 fish, e.g. event 1 (Fig.5). Lu et al (2016) showed that co-precipitation of P with metal oxides was stimulated by periphytic
499 biofilm activity that increased the water pH. Consistently, a relatively higher pH was also observed in our spring monthly
500 samples (Fig.6).

501 From the late autumn onwards, turbidity and total Fe concentrations substantially increased compared to the rest of the time
 502 (Fig.2, p value < 0.001 for turbidity and = 0.02 for Fe). Turbidity peaked first at 1800 FNU and stayed at a plateau of ~200
 503 NFU during the rest of the cold and wet season. Total Fe in the water column reached to 6 mg L⁻¹ from below 1 mg L⁻¹. During
 504 this period the water turned brownish and transparency declined (Fig.6). Iron-rich particles are the most likely source of
 505 turbidity in freshwater (Lyvén et al., 2003; Gunnars et al., 2002; and Lofts et al, 2008). The suspension of these brownish iron
 506 colloids was likely stabilised by the presence of the dissolved organic matter (Mosley et al., 2003; Van der Grift et al., 2014),
 507 which (DOC) increased up to 18~33 mg L⁻¹ during events (Supplementary information Figure S4). In the late autumn, the
 508 anoxic/oxic interface shifts from the sediment into the water column and so does the locus of colloid formation. The ditch
 509 sediment, which had benthic algae activity releasing O₂ during spring and summer, became anoxic in the fall by the upwelling
 510 of the anoxic groundwater. The anoxic seepage occurs year-round, but the production of oxygen by the benthic algae creates
 511 an anoxic-oxic transition at the water-sediment interface, which leads to iron hydroxides precipitation in the slimy layer at the
 512 bottom that disappears after the algae die off. As a consequence, Fe oxidation moved into the water column where the
 513 conditions were relatively oxic (Van der Grift et al., 2014). Nevertheless, there was probably still enough Fe or other mineral
 514 oxides, such as aluminum hydroxide (Kopáček et al., 2005), binding capacity in the sediment for the fixation of P, as P
 515 concentrations remained low during this first turbidity peak. We suggest that the turbidity peak of 1800 FNU is caused by the
 516 mineralisation of the benthic algae once they die off when light and temperature conditions decrease, combined with the shift
 517 of ironhydroxide formation from the sediment-water interface to the water column. The latter process continues through the
 518 whole winter season, until primary production restarts in spring (Figure 7).
 519 During winter, temperatures were below 5°C, pH values were relatively lowered, and TP achieved its peak concentrations
 520 (Fig.2D). During this period, iron reduction in the sediments continued, P bounded to iron oxides gradually got released along
 521 with reduced iron (Li et al., 2016). In the water column, reduced iron was oxidized but much slower than during spring-autumn
 522 due to the lower temperatures (Van der Grift et al., 2014), and dissolved P was incorporated in iron flocs with the result that
 523 particulate P concentrations and turbidity became high (Table S1, R² for Fe~turbidity 0.81, TP~Fe 0.65; Table S2, Fe~turbidity:
 524 R² = 0.72, , TP grab~Fe 0.79; Yu et al., 2019).

525 4.4 Process synthesis

526 With the presence of benthic algae, abundant organic matter and bacteria, the sediment functions as an active environment for
 527 biotic processes (such as primary production and nitrification-denitrification-anammox) and abiotic processes (such as iron
 528 oxidation). Figure 7 shows a conceptual diagram for the N and P dynamics in this lowland urban catchment during the four
 529 seasons which summarizes our hypotheses about the functioning of the system.



534 **Spring:** The improved light (and temperature) conditions stimulated primary production and nutrient uptake (N, P, Si) by
535 phytoplankton and benthic algae. The resulting oxygen production caused oxidation of reduced iron from groundwater and the
536 formation of iron oxides at the sediment surface. P was mostly bounded to this particulate iron instead of being released into
537 the upper water layer. In this period turbidity was relatively low, but suspended solids reached a high concentration due to the
538 phytoplankton.

539 **Summer:** N and P were still being removed by biological processing, in particular by benthic algae. Phytoplankton biomass
540 decreased because of competition for N or grazing activity. Benthic algae produced O₂, which in turn was used to oxidize all
541 reduced iron reaching the sediment-water interface and P was still retained by iron hydroxides in the sediment. The water
542 column was transparent (low TP and phytoplankton biomass) and relatively low in oxygen due to the continuous supply of
543 anoxic groundwater, the mere absence of O₂-rich runoff, the oxidation process of Fe(II) and possibly by microbial organic
544 matter decomposition during warm periods with relatively stagnant water.

545 **Late autumn:** Biological activity declined (colder and less light), and more NH₄ reached the water column. Moreover, the
546 redox zone moved from the sediment-water interface into the water column (Van der Grift et al. 2014, 2016); the oxidation of
547 Fe in the water column caused a peak of turbidity. P was still sequestered to minerals in the sediment.

548 **Winter:** During winter, NH₄ and TP showed the highest concentrations because of low biological activity. Iron oxides in the
549 sediment dissolved under reductive and organic matter abundant conditions and released Fe²⁺ and P into the water column
550 increasing P concentrations therein. NH₄ and EC dynamics were primarily governed by the conservative mixing between
551 groundwater and precipitation/runoff.

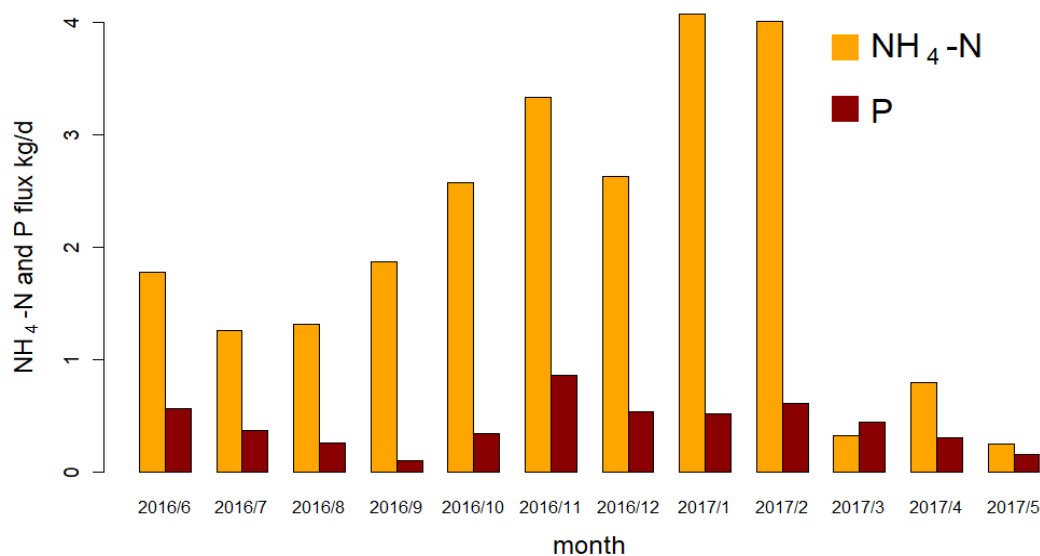
552 **4.5 Event scale N and P dynamics**

553 At the event scales, NH₄ and EC were reduced by dilution from precipitation/runoff. For P and turbidity there was no clear
554 relation to precipitation events, except for events in late autumn and winter (e.g. Figure 4, event 3). The responses to
555 precipitation and pumping events were different from those reported in the literature. Rozemeijer et al. (2010b) studied an
556 agricultural catchment and found that rainfall events led to NO₃ decreases and P increases. Miller et al. (2016) observed NO₃
557 decreases during large discharges in an urban catchment. The lowering of turbidity in our urban catchment during the dilution
558 periods that was associated with the winter events 3 ~~and~~ differs from the observations in literature (van der Grift et al., 2014,
559 Rozemeijer et al., 2010b). In agriculture areas, turbidity usually peaks in response to rainfall events due to erosion and
560 remobilization of sediments. In an urban, paved environment erosion may be limited and runoff water has a low turbidity.
561 Moreover, in the case of turbid pre-event conditions, fresh precipitation water flushes away this turbid water. In addition, Yu
562 et al. (2019) showed that precipitation runoff delivers particles and O₂ to the ditches. We suggest that this accelerates the
563 further aggregation of the iron complexes; the resulting larger particles more readily settle to the bottom, causing a reduction
564 of turbidity during the events itself (Fig. 4, EC dilution part of events 3 and 4).

565 In artificial lowland catchments, water systems are intensively regulated by pumping activity to prevent flood and drought.
566 However, there is a substantial lack of knowledge about the possible consequences of such regulation on aquatic ecology and
567 water quality. Peaks in P and turbidity by the activation of pumps was observed by Van der Grift et al. in their high frequency
568 monitoring campaign in an agriculture lowland polder (Van der Grift et al., 2014 & 2016). This type of event scale dynamics
569 would be easily missed in a daily or lower frequency sampling schedule, especially because pumping occurs almost solely
570 overnight in our regulated catchments. As such, only a sampling schedule with 7 hours intervals (e.g. Neal et al. 2011) or high-
571 frequency monitoring is able to catch the short-term dynamics (Van Geer et al. 2016).

572 Contrary to the findings of Van der Grift et al. (2014, 2016), the effects of pumping activity on N, P and turbidity dynamics
573 were variable, depending on the season. During the phytoplankton bloom in spring, activation of pumps resulted in flushing
574 and as a result reduced turbidity during the event (Fig. 5 event 4). Consequently, phytoplankton was transferred to the
575 downstream channel and added to the total N pool in that system. In summer (Fig.5 event 1), the dead detritus and the layer of

576 iron compounds at the sediment surface were easily resuspended and contributed to turbidity peaks at the beginning of the
 577 pumping, but the materials also re-sedimented almost immediately once the flow reached stability. Resuspension also resulted
 578 in an increase of NH_4 in the water column which then was being pumped out (Fig.5 event 1). During late autumn, we observed
 579 that the water was highly turbid (see also Yu et al. 2019) which we suggest to be caused by the formation of iron hydroxide
 580 colloids in the water column, which is supported by correlations between Fe-grab and Turbidity ($R^2= 0.72$, Table S2). We
 581 explain the reduced turbidity after a precipitation event as a result of the activation of the pumps which caused the export of
 582 the turbid water towards the receiving boezem in combination with aggregation of iron hydroxides in the water column and
 583 subsequent settling of the aggregates due to the supply of new O_2 -rich water (Fig.5 event 2, see also Van der Grift, et al., 2014).
 584 Moreover, NH_4 increased again by the pumping activity and was transferred downstream (Fig.5 event 2). The eventual impact
 585 of regulation of the Geuzenveld water system turns the pumping discharge into a point source for nutrients to downstream
 586 water bodies as shown in Figure 8.



587
 588 **Figure 8 Average daily NH_4 -N and P flux (kg per day) in each month in the discharge (calculated from the continuous**
 589 **measurements) of polder Geuzenveld from June 2016 to May 2017.**

591 Fluxes of N and P were highest during winter (Fig 6). These high fluxes are caused not only by the more frequent pumping
 592 activity, but also by the higher concentration of N and P in the water column in winter. In the time series data, NH_4 (the major
 593 form of N), had concentrations above 2.4 mg N L^{-1} (the local environmental quality standard (EQS) for N-total), in all seasons
 594 except spring. NH_4 concentrations even reached up to 6.5 mg L^{-1} . TP concentrations were constantly higher than 0.15 mg P L^{-1}
 595 (the local EQS); during winter it was always over 1 mg P L^{-1} . Although the NH_4 flux in the discharge was very low in spring
 596 (Fig.8), the actual total N flux might have been much higher, as organic N (phytoplankton) was the major form of TN instead
 597 of NH_4 during this period (Fig.6 NH_4/N and organic-N/TN). Therefore, even though water authority measures have been
 598 effective in controlling the water quantities in the polder, it had unanticipated impact on nutrients export to the downstream
 599 water bodies. In order to prevent eutrophication in the urban waters, nutrient rich discharge from these areas is exported directly
 600 to the North-Sea Canal and to the North Sea.

602 4.6 Implications for urban water management in low lying catchments

603 This study demonstrated high frequency monitoring technology to be an effective tool for understanding the complex water
 604 quality dynamics. Investment in high frequency monitoring would greatly benefit the management of urban lowlands with
 605 substantial groundwater seepage by elucidating the principle biogeochemical processes and nutrient temporal patterns for

606 realizing efficient mitigation and control of eutrophication. For example, redirecting the drain water effluent into constructed
607 wetlands could be considered as a mitigation measure in low lying areas with artificial water systems that resemble the
608 Amsterdam region, e.g. in cities such as New Orleans, Shanghai and Dhaka (Li et al., 2009; Nahar et al., 2014; Jones et al.,
609 2016; Stahl, 2019). Centralizing the treatment of discharge water is also recommended, for instance by harvesting N as
610 phytoplankton from the discharge during spring, or filtrating P at the pumping station during winter. Measures that artificially
611 increase oxygen concentrations in the waters, such as the inlet of oxygen rich water, aeration by fountains or the artificial
612 introduction of grazers or macrophytes may be considered to improve the ecological status of these urban waters. Moreover,
613 aeration of the water in summer and autumn would possibly enhance processes such as coupled-nitrification-denitrification
614 and anammox, eventually converting NH_4 to N_2 , before the water is discharged to downstream waters. Importantly, before the
615 application of any measures or maintenance in urban low-lying catchments, managers should evaluate the potential effects on
616 the biological and chemical resilience, e.g. dredging of a layer with abundant benthic activity might destroy an important buffer
617 to nutrients in growing seasons, especially P.

618 In this study, we focused on the analysis of the temporal patterns of water composition and on the deduction of the potential
619 biogeochemical processes. Detailed studies about these processes and the biotic communities at the sediment-water interface
620 were outside of the scope of this paper. A comprehensive study on the sediment-water interface would be necessary to further
621 increase our knowledge on the role of the benthic zone in attenuating N and P seeping up from groundwater. Besides, further
622 research would need to consider the optimal physical dimensions of water courses and drain configurations, as to benefit the
623 ecological status of urban waters that are prone to nutrient-rich groundwater seepage.

624

625 5. Conclusions

626 This study aimed at improving our understanding of the mechanisms that control the temporal patterns of nutrients and other
627 water quality parameters in an urban catchment. Time series of EC, NH_4 , TP, and turbidity were obtained by applying a high
628 frequency monitoring technology for one year (May 2016 to July 2016). Observed EC, NH_4 and TP could only partly be
629 explained by conservative mixing of groundwater and precipitation components. In particular, N and P fluxes in the shallow
630 ditches were also impacted by biogeochemical processes, such as primary production and iron redox transformations.

631 (1) NH_4 , the dominant form of N in surface water, originates primarily from groundwater seepage, and concentrations
632 are lowered by primary producers (phytoplankton and benthic algae) in the growing season. High algal biomass was
633 also clear from high chlorophyll-a and suspended solids in the water column.

634 (2) TP showed high concentrations in winter, but relatively low concentrations in other seasons. Iron redox chemistry
635 was the principle process controlling the P dynamics in shallow groundwater fed ditches. P dynamics may also have
636 been partly influenced by primary production which consumes P for growth and at the same time produces O_2
637 influencing the redox status in the sediments and in the water column.

638 (3) High turbidity levels occurred in the late autumn and winter, mostly in the form of iron hydroxides. It resulted from
639 a shift of the anoxic/oxic interface where the formation of iron hydroxides moves from the sediment towards the
640 water column.

641 (4) Water pumped from the polder to downstream water bodies was rich in NH_4 from summer to winter, but rich in
642 organic N in the form of algae during spring. P leaves the polder mainly during the winter season when it is released
643 from the sediment and exported mostly in the form of P sorbed to $\text{Fe}(\text{OH})_3$ colloids and as dissolved P.

644 (5) Precipitation diluted concentrations of most water quality parameters, but delivered O_2 to the water column, and in
645 that way indirectly affected P and turbidity by intensifying iron oxidation and precipitation.

646 (6) Unlike many other natural and artificial catchments, rainfall and pumping events did not increase turbidity or TP
647 concentrations at the short time scale, rather reduced turbidity and TP because of enhanced iron hydroxide
648 precipitation due to oxygen inputs by runoff.

649 Our understanding of the N and P dynamics in this low-lying urban catchment may contribute to the development of effective
650 water management strategies that reduce eutrophication conditions in both the urban polders and the downstream waters.
651 Drainage of very low-lying areas (for use as residential and/or agricultural areas) not only increases pumping costs, but can
652 also result in difficult to manage water quality conditions. Controlling the source, redirecting and utilizing the drainage water
653 might be strategies to reduce the input of N and P from groundwater into surface water. In addition, we showed that in lowland
654 urban areas with high seepage rates the reactivity of the stream bed sediments largely controls water quality of surface waters
655 and thus should be managed with care when cleaning the surface water systems.

656 **Acknowledgements**

657 This work was funded through China scholarship council (no. 201309110088) and supported by Waternet, the Strategic
658 Research Funding of TNO and Deltares. We highly appreciate the help and support from our Waternet co-workers: Eelco
659 Wiebenga, Henk Molenaar, Sonja Viester, Laura Moria, and Frank Smits.

660 **Code/data availability:** The code scripts and datasets related to this paper are available on request to Liang Yu, contact is
661 xiaobaidrawing@gmail.com.

662
663 **Author contribution:** Maarten Ouboter, Joachim Rozemeijer, and Hans Peter Broers funded this research. Hans Peter Broers
664 and Joachim Rozemeijer designed the field work. Liang Yu carried out the field work and the data collection, analysis,
665 visualization, discussion, and the writing of the manuscript, under the supervision of Hans Peter Broers and Joachim
666 Rozemeijer before 2019, Ype van der Velde as the main supervisor since 2019. All the authors participated the discussion of
667 the data analysis results, and helped prepare the manuscript.

668
669 **Competing interests:** The authors declare that there is no conflict of interest.

670 **References**

- 671 Audet J., Zak D., Bidstrup J., and Hoffmann C.C.. Nitrogen and phosphorus retention in Danish restored wetlands. Royal
672 Swedish Academy of Sciences, 1-13, 2019.
- 673 Bunch N.D. and Bermot M.J.. Nitrate and ammonium uptake by natural stream sediment microbial communities in response
674 to nutrient enrichment. *Research in Microbiology*, 163(2): 137-141, 2012.
- 675 Beusen A.H.W., Bouwman A.F., van Beek L.P.H., Mogollón J.M., and Middelburg J.J.. Global riverine N and P transport to
676 ocean increased during the 20th century despite increased retention along the aquatic continuum. *Biogeosciences*. 13: 2441-
677 2451, 2016.
- 678 Bieroza M.Z., Heathwaite A.L., Bechmann M., Kyllmar K., and Jordan P.. The concentration-discharge slope as a tool for
679 water quality management. *Science of the Total Environment*, 630: 738-749, 2018.
- 680 Baken S., Sjostedt C., Gustafsson J.P., Seuntjens P., and Desmet N.. Characterisation of hydrous ferric oxides derived from
681 iron-rich groundwaters and their contribution to use suspended sediment of streams. *Applied Geochemistry*, 39: 59-68, 2013.
- 682 Cavaliere E. and Baulch H.M.. Winter nitrification in ice-covered lakes. *PLoS ONE*, 14(11): e0224864, 2019.
- 683 Chen M., Ding S., Chen X., Sun Q., Fan X., Lin J., Ren M., Yang L., and Zhang C.. Mechanisms driving phosphorus release
684 during algal blooms based on hourly changes in iron and phosphorus concentrations in sediments. *Water Research*, 133: 153-
685 164, 2018.

686 Díaz P., Stanek P., Frantzeskaki N., and Yeh D.H.. Shifting paradigms, changing waters: Transitioning to integrated urban
687 water management in the coastal city of Dunedin, USA. *Sustainable Cities and Society*, 26: 555-567, 2016.

688 Duncan J.M., Welty C., Kemper J.T., Groffman P.M., and Band L.E.. Dynamics of nitrate concentration-discharge patterns in
689 an urban watershed. *Water Resources Research*, 53: 7349-7365, 2017.

690 Eggimann S., Mutzner L., Wani O., Schneider M.Y., Spuhler D., de Vitry M.M., Beutler P., and Maurer M.. The Potential of
691 Knowing More: A Review of Data-Driven Urban Water Management. *Environmental Science & Technology*, 51: 2538-2553,
692 2017.

693 Filippelli M.G.. The global phosphorus cycle: Past, present, and future. *Elements*, 4(2): 89-95.

694 Fletcher T.D., Shuster W., Hunt W.F., Ashley R., Butler D., Arther S., Trowsdale S., Barraud S., Semadeni-Davies A.,
695 Bertrand-Krajewski J.L., Mikkelsen P.S., Rivard G., Uhl M., Dagenais D., and Viklander M.. SUDS, LID, BMPs, WSUD
696 and more – The evolution and application of terminology surrounding urban drainage. *Urban Water Journal*, 12(7): 525-542,
697 2015.

698 Griffioen J.. Extent of immobilisation of phosphate during aeration of nutrient-rich, anoxic groundwater. *Journal of Hydrology*,
699 320 (3-4): 359-369, 2006.

700 Gunnars A., Blomqvist S., Johansson P., and Andersson C.. Formation of Fe (III) oxyhydroxide colloids in freshwater and
701 brackish seawater, with incorporation of phosphate and calcium. *Geochim. Cosmochim. Acta*, 66 :745-758, 2002.

702 Genkai-Kato M., Vadeboncoeur, Liboriussen L., and Jeppesen E.. Benthic-planktonic coupling, regime shifts, and whole-lake
703 primary production in shallow lakes. *Ecology*, 93(3): 619-631, 2012.

704 Hartwig E.O.. Factors affecting respiration and photosynthesis by the benthic community of a subtidal siliceous sediment.
705 *Marine Biology*, 46: 283-293, 1978.

706 Hansson L.A.. Effects of competitive interactions on the biomass development of planktonic and periphytic algae in lakes.
707 *Limnology and Oceanography*, 33(1): 121-128, 1988. Henry J.C. and Fisher S.G.. Spatial segregation of periphyton
708 communities in a desert stream: causes and consequences for N cycling. *Journal of The North American Benthological Society*,
709 22 (4): 511-527, 2003.

710 He S. and Xu Y.J.. Three decadal inputs of nitrogen and phosphorus from four major coastal rivers to the summer hypoxic
711 zone of the northern Gulf of Mexico. *Water, Air, and Soil Pollution*, 226: 311, 2015.

712 Jäger C.G. and Borchardt D.. Longitudinal patterns and response lengths of algae in riverine ecosystems: A model analysis
713 emphasizing benthic-pelagic interactions. *Journal of Theoretical Biology*, 442: 66-78, 2018.

714 Jäger C.G., Hagemann J., and Borchardt D.. Can nutrient pathways and biotic interactions control eutrophication in riverine
715 ecosystems? Evidence from a model driven mesocosm experiment. *Water Research*, 115: 162-171, 2017.

716 [Jones C.E., An K., Blom R.G., Kent J.D., Ivins E.R., and Bekaert D.. Anthropogenic and geologic influences on subsidence
717 in the vicinity of New Orleans, Louisiana. *JGR Solid Earth*, 121\(5\): 3867-3887, 2016.](#)

718 Kuenen J.. Anammox bacteria: from discovery to application. *Nature Reviews Microbiology*, 6: 320-326, 2008.

719 Kopáček J., Borovec J., Hejzlar J., Ulrich K., Norton S.A., and Amirbahman A.. Aluminum control of phosphorus sorption by
720 lake sediments. *Environmental Science & Technology*, 39 (22): 8784-8789, 2005.

721 Kleeberg A., Hupfer M., and Gust G.. Phosphorus entrainment due to resuspension in a lowland river, Spree, NE Germany-A
722 laboratory microcosm study. *Water, Air, and Soil Pollution*, 183(1-4): 129-142, 2007.

723 Kabenge M., Wang H., and Li F.. Urban eutrophication and its spurring conditions in the Murchison Bay of Lake Victoria.
724 *Environmental Science and Pollution Research*, 23: 234-241, 2016.

725 Lijklema L.. Nutrient dynamics in shallow lakes: effects of changes in loading and role of sediment-water interactions.
726 *Hydrobiologia*, 275/276: 335-348, 1994.

727 [Li X., Chen M., and Anderson B.C.. Design and performance of a water quality treatment wetland in a public park in Shanghai,
728 China. *Ecological Engineering*, 35: 18-24, 2009.](#)

729 Le Moal M., Cascuel-Oudoux C., Menesguen A., Souchon Y., Etrillard C., Levain A., Moatar F., Pannard A., Souchu P.,
730 Lefebvre A., and Pinay G.. Eutrophication: A new wine in an old bottle. *Science of the Total Environment*, 651: 1-11, 2019.

731 Lyvén B., Hassellöv M., Turner D.R., Haraldsson C., and Andersson K.. Competition between iron- and carbon-based colloidal
732 carries for trace metals in a freshwater assessed using flow field-flow fractionation coupled to ICPMS. *Geochimica et*
733 *Cosmochimica Acta*, 67(20): 3791-3802, 2003.

- 734 Li H., Song C.L., Cao X.Y., and Zhou Y.Y.. The phosphorus release pathways and their mechanisms driven by organic carbon
735 and nitrogen in sediments of eutrophic shallow lakes. *Science of the Total Environment*, 572: 280-288, 2016.
- 736 Lofts S., Tipping E., and Hamilton-Taylor J.. The Chemical Speciation of Fe(III) in Freshwaters. *Aquatic Geochemistry*, 14(4):
737 337-358, 2008.
- 738 Lu H., Wang J., Li J., Shao H., and Wu Y.. Periphytic biofilm: A buffer for phosphorus precipitation and release between
739 sediments and water. *Chemosphere*, 144: 2058-2064, 2016.
- 740 Middelburg J.J.. *Marine Carbon Biogeochemistry - A Primer for Earth System Scientists*. Springer Briefs in Earth System
741 Sciences. Switzerland, 2019.
- 742 McGlathery K.J., Anderson I.C., and Tyler A.C.. Magnitude and variability of benthic and pelagic metabolism in a temperate
743 coastal lagoon. *Marine Ecology Progress Series*, 216: 1-15, 2001.
- 744 Mosley L.M., Hunter K.A., and Ducker W.A.. Forces between Colloid Particles in Natural Waters. *Environmental Science &*
745 *Technology*, 37 (15): 3303-3308, 2003
- 746 Middleburg J.J. and Nieuwenhuize J.. Uptake of dissolved inorganic nitrogen in turbid, tidal estuaries. *Marine Ecology*
747 *Progress Series*, 192: 79-88, 2000.
- 748 Miller M.P., Tesoriero A.J., Capel P.D., Pellerin B.A., Hyer K.E., and Burns D.A.. Quantifying watershed-scale groundwater
749 loading and instream fate of nitrate using high-frequency water quality data. *Water Resources Research*, 52: 330-347, 2016.
- 750 Mulder A., van de Graaf A.A., Robertson L.A., and Kuenen J.G.. Anaerobic ammonium oxidation discovered in a denitrifying
751 fluidized bed reactor. *FEMS Microbiology Ecology*, 1(16): 177-184, 1995.
- 752 Nyenje P.M., Foppen J.W., Uhlenbrook S., Kulabako R., and Muwanga A.. Eutrophication and nutrient release in urban areas
753 of sub-Saharan Africa-A review. *Science of the Total Environment*, 408: 447-455, 2010.
- 754 Neal, C., Reynolds, B., Norris, D., Kirchner, J. W., Neal, M., Rowland, P., Wickham H., Harman S., Armstrong L., Sleep D.,
755 Lawlor, A., Woods C., Williams B., Fry M., Newton G., Wright D.. Three decades of water quality measurements from the
756 Upper Severn experimental catchments at Plynlimon, Wales: an openly accessible data resource for research, modelling,
757 environmental management and education. *Hydrological Processes*, 25(24), 3818-3830, 2011.
- 758 Nizzoli D., Welsh D.T., and Viaroli P.. Denitrification and benthic metabolism in lowland pit lakes: The role of trophic
759 conditions. *Science of the Total Environment*, 703: 134804, 2020.
- 760 [Nahar, M.S., Zhang, J., Ueda, A. et al. Investigation of severe water problem in urban areas of a developing country: the case](#)
761 [of Dhaka, Bangladesh. *Environmental Geochemistry and Health*, 36: 1079-1094, 2014.](#)
- 762 Painter H.A.. A review of literature on inorganic nitrogen metabolism in microorganisms. *Water Research*, 4: 393-450, 1970.
- 763 Pasterank A., Hillebrand H., and Flöder S.. Competition between benthic and pelagic microalgae for phosphorus and light-
764 long-term experiments using artificial substrates. *Aquatic Sciences*, 71: 238-249, 2009.
- 765 Putt A.E., MacIsaac E.A., Herunter H.E., Cooper A.B., and Selbie D.T.. Eutrophication forcings on a peri-urban lake
766 ecosystem: Context for integrated watershed to airshed management. *PLoS ONE*, 4(7): e0219241, 2019.
- 767 Paerl H.W., Scott J.T., McCarthy M.J., Newell S.E., Gardner W.S., Havens K.E., Hoffman D.K., Wilhelm S.W., and
768 Wurtsbaugh W.A. It Takes Two to Tango: When and Where Dual Nutrient (N & P) Reductions Are Needed to Protect Lakes
769 and Downstream Ecosystems. *Environmental Science & Technology*, 50: 10805-10813, 2016.
- 770 Rozemeijer J.C. and Broers H.P.. The groundwater contribution to surface water contamination in a region with intensive
771 agricultural land use (Noord-Brabant, The Netherlands). *Environmental Pollution*. 148(3): 695-706, 2007.
- 772 Rozemeijer J.C., van der Velde Y., van Geer F.C., Bierkens M.F.P., and Broers H.P.. Direct measurements of the tile drain
773 and groundwater flow route contributions to surface water contamination: From field-scale concentration patterns in
774 groundwater to catchment-scale surface water quality. *Environmental Pollution*, 158: 3571-3579, 2010a.
- 775 Rozemeijer J.C., van der Velde Y., van Geer F.C., de Rooij G.H., Torfs P.J.J.F. and Broers H.P.. Improving load estimates for
776 NO₃ and P in surface water by characterizing the concentration response to rainfall events. *Environmental Science &*
777 *Technology*, 44 (16): 6305-6312, 2010b.
- 778 Rode M., Wade A.J., Cohen M.J., Hensley R.T., Michael J.B., Kirchner J.W., Arhonditsis G.B., Jordan P., Kronvang B.,
779 Halliday S.J., Skeffington R., Rozemeijer J., Aubert A.H., Rinke K., and Jomaa S.. Sensors in the stream: the high-frequency
780 wave of the present. *Environmental Science & Technology*, 50: 10297-10307, 2016.
- 781 Scheffer, M.. *Ecology of shallow lakes*, 1st edition. London: Chapman & Hall, 1998.

782 [Stahl M.O.. Groundwater pumping is a significant unrecognized contributor to global anthropogenic element cycles.](#)
783 [Groundwater. 57\(3\) : 455-464, 2019.](#)

784 Spears B.M., Carvalho L., Perkins R., Kirika A., and Paterson D.M.. Sediment phosphorus cycling in a large shallow lake:
785 spatio-temporal variation in phosphorus pools and release. *Hydrobiologia*, 584: 37-48, 2007.

786 Smolders A.J.P., Lamers L.P.M., Lucassen E.C.H.E.T., Van Der Velde G., and Roelofs J.G.M.. Internal eutrophication: How
787 it works and what to do about it—a review. *Chemistry and Ecology*, 22(2): 93-111, 2006.

788 Strayer D.L., Pace M.L., Caraco N.F., Cole J.J., and Findlay S.E.G.. Hydrology and grazing jointly control a large-river food
789 web. *Ecology*, 89(1): 12-18, 2008.

790 Thamdrup B. and Dalsgaard T.. Production of N₂ through anaerobic ammonium oxidation coupled to nitrate reduction in
791 marine sediments. *Applied and Environmental Microbiology*, 68(3): 1312-1318, 2002.

792 Toor G.S., Occhipinti M.L., Yang Y.Y., Majcherek T., Haver D., and Oki L.. Managing urban runoff in residential
793 neighbourhoods: Nitrogen and phosphorus in lawn irrigation driven runoff. *PLoS ONE*, 12(6): e0179151, 2017.

794 Van der Grift, B., Broers, H.P., Berendrecht, W., Rozemeijer, J., Osté, L., and Griffioen, J.. High-frequency monitoring reveals
795 nutrient sources and transport processes in an agriculture-dominated lowland water system. *Hydrology and Earth System
796 Sciences*, 20(5): 1851-1868, 2016.

797 Van Geer F.C., Kronvang B., and Broers H.P.. High-resolution monitoring of nutrients in groundwater and surface waters:
798 process understanding, quantification of loads and concentrations, and management applications. *Hydrology and Earth System
799 Sciences*, 20: 3619-3629, 2016.

800 Van der Grift B., Osté L., Schot P., Kratz A., van Popta E., Wassen M., and Griffioen J.. Forms of phosphorus in suspended
801 particulate matter in agriculture-dominated lowland catchments: Iron as phosphorus carrier. *Science of The Total Environment*,
802 631-632: 115-129, 2018.

803 Van der Velde Y., Rozemeijer J.C., de Rooij G.H., van Geer F.C., Broers H.P.. Field-scale measurements for separation of
804 catchment discharge into flow route contribution. *Vadose Zone Journal*, 9(1): 25-35, 2010.

805 Van der Grift B., Rozemeijer J.C., Griffioen J., and van der Velde Y.. Iron oxidation kinetics and phosphate immobilization
806 along the flow-path from groundwater into surface water. *Hydrology and Earth System Sciences*, 18: 4687-4702, 2014.

807 Wilczak A., Jacangelo, J.G., Marcinko J.P., Odell L.H., and Kirmeyer G.J.. Occurrence of nitrification in chloraminated
808 distribution systems. *Journal AWWA*, 88(7): 74-85, 1996.

809 Wang T., Liu G., Gao L., Zhu L., Fu Q., and Li D.. Biological and Nutrient Responses to a Typhoon in the Yangtze Estuary
810 and the Adjacent Sea. *Journal of Coastal Research*, 32(2): 323-332, 2016.

811 Walsh C.J., Roy J.W., Feminella J.W., Cottingham P.D., Groffman P.M., and Morgan II R.P.. The urban stream syndrome:
812 current knowledge and the search for a cure. *Journal of The North American Benthological Society*, 24(3): 706-732, 2005.

813 Wriedt, G., Spindler J., Neef T., Meißner R., and Rode M.. Groundwater dynamics and channel activity as major controls of
814 in-stream nitrate concentrations in a lowland catchment system? *Journal of Hydrology*, 343: 154–168, 2007.

815 Yu L., Rozemeijer J.C., van Breukelen B.M., Ouboter M., van der Vlugt C., and Broers H.P.. Groundwater impacts on surface
816 water quality and nutrient loads in lowland polder catchments: monitoring the greater Amsterdam area. *Hydrology and Earth
817 System Sciences*, 22:487-508, 2018.

818 Yu L., Rozemeijer J.C., van der Velde Y., van Breukelen B.M., Ouboter M., and Broers H.P.. Urban hydrogeology: Transport
819 routes and mixing of water and solutes in a groundwater influenced urban lowland catchment. *Science of the Total
820 Environment*, 678: 288-300, 2019.

821 Yang Y.Y. and Toor G.S.. Stormwater runoff driven phosphorus transport in an urban residential catchment: Implications for
822 protecting water quality in urban watersheds. *Scientific Reports*, 8: 11681, 2018. doi: 10.1038/s41598-018-29857-x

823 Zhu W.X., Dillard N.D., and Grimm N.B.. Urban nitrogen biogeochemistry: status and processes in green retention basins.
824 *Biogeochemistry*, 71: 177-196, 2004.

825 Zhang W., Jin X., Meng X., Tang W., and Shan B.. Phosphorus transformations at the sediment-water interface in shallow
826 freshwater ecosystems caused by decomposition of plant debris. *Chemosphere*, 201: 328-334, 2018.

827 Zhang X. and Mei X.. Effects of benthic algae on release of soluble reactive phosphorus from sediments: a radioisotope tracing
828 study. *Water Science and Engineering*, 8(2): 127-131, 2015.

829 Zhou L., Wang S., Zou Y., Xia C., and Zhu G.. Species, abundance and function of ammonia-oxidizing Archaea in inland
830 waters across China. *Scientific Reports*, 5: 15969, 2015.